2015

Doppler spread estimation in high mobility wireless communications

Zichen Wang
University of Wollongong

Doppler Spread Estimation in High Mobility Wireless Communications

A thesis submitted in partial fulfilment of the requirements for the award of the degree

Master of Engineering by Research

from

UNIVERSITY OF WOLLONGONG

by

Zichen Wang

School of Electrical, Computer and Telecommunications Engineering

March 2015

Statement of Originality

I, Zichen Wang, declare that this thesis, submitted in partial fulfilment of the requirements for the award of Master of Engineering - Research, in the School of Electrical, Computer and Telecommunications Engineering, University of Wollongong, is wholly my own work unless otherwise referenced or acknowledged. The document has not been submitted for qualifications at any other academic institution.

Zichen Wang

March 26, 2015

Contents

List of Figures

List of Tables

Abbreviations

ACF	Autocorrelation function
AR	Autoregressive
AR(1)	First order autoregressive
AWGN	Additive white Gaussian noise
EM	Expectation-maximization
FFG	Forney-style factor graph
GMP	Gaussian message passing
i.i.d.	Independent and identically distributed
I/Q	In-phase/quadrature-phase
ISI	Inter-symbol interference
LCR	Level-crossing rate
LLF	Log-likelihood function
LMMSE	Linear minimum mean square error
LOS	Line-of-sight
ML	Maximum likelihood
MSE	Mean square error
NMSE	Normalized mean square error
PDF	Probability density function
PSD	Power spectrum density
RMS	Root mean square
SC	Sample covariance
SML	Suboptimal Maximum Likelihood
SNR	Signal-to-noise ratio
WSS	Wide sense stationary
ZCP	Zero-crossing point

Abstract

Wireless communication systems have experienced phenomenal growth over the last three decades. Tremendous research efforts have been devoted, and many important developments have been made. Future wireless communication systems aim at providing reliable data transmission even under high mobility scenarios. One of the challenging issues is the large Doppler spread, which is caused by the high mobility of a wireless terminal and may lead to severe communication performance loss. Doppler spread is a measure of spectral broadening of the rate of change in a mobile fading channel which is proportional to the mobile speed. As Doppler spread is a significant parameter of the mobile channel, it is important to a number of wireless mobile applications which require the knowledge of the fading rate of channel variations or the mobile speed. Therefore, the large Doppler spread in high mobility wireless communication systems cannot be negligible anymore and an accurate estimate of Doppler spread is imperative to develop future mobile communication systems for high speed vehicles. The objective of this thesis is to design effective algorithms for Doppler spread estimation in high mobility wireless communication scenarios.

Many approaches have been proposed for Doppler spread estimation. The op-

timal Doppler spread estimation is based on the maximum likelihood principle, which usually involves exorbitant complexity. Other Doppler spread estimation approaches, such as the level crossing rate based approach and the covariance based approach, are with low complexity, but they need a large number of observations and their performance degradation exists in either low Doppler spread range or high Doppler spread range.

As the knowledge of Doppler spread can be used to characterise the time variation of fading channels, it can be employed to enhance channel estimation performance. Many Doppler spread estimation approaches are based on the channel estimates, while the channel coefficients are assumed to be known at the receiver. The mutual dependence of channel estimation and Doppler spread estimation motivates joint Doppler spread and channel estimation in order to achieve better performance.

We propose a new joint Doppler spread and channel estimation approach for Rayleigh fading channels through an iterative process between a Doppler spread estimator and a channel estimator. The proposed Doppler spread estimator is based on the autocorrelation function (ACF) of the estimated channel coefficients, where we devise an ACF lag selection mechanism to maximise the performance of Doppler spread estimation. We use a Forney-style factor graph to represent the fading channel with a first order autoregressive (AR(1)) model and implement a Gaussian message passing (GMP) based channel estimator for Doppler spread estimation, where the AR(1) model coefficients are optimised. Compared to existing joint Doppler spread and channel estimation approaches, the proposed approach achieves similar or better performance with lower complexity.

We also propose an expectation-maximization (EM) based time-varying channel estimation approach. It has been shown that the EM algorithm may be viewed as message passing in factor graphs, and for a linear Gaussian system with unknown parameters, the EM algorithm may be implemented by the GMP techniques. With a Forney-style factor graph representation of the fading channel approximated by an AR(1) model, we devise a low-complexity EM-GMP based approach to joint estimate the channel coefficients and the AR(1) model coefficients, where the Doppler spread can be extracted from the estimated AR(1) model coefficients. The proposed EM-GMP based approach has similar complexity per iteration as the conventional EM based approach, but it significantly outperforms the conventional EM based approach in terms of convergence rate, especially in low Doppler spread range.

Acknowledgments

First of all, I would express my deepest gratitude to my supervisor, Dr. Qinghua Guo, for his patient guidance, constructive suggestions and constant encouragements through my master studies. Dr. Guo has set a good example for me in both research and life.

Special thanks goes to my co-supervisors, Dr. Sheng Tong and Prof. Jiangtao Xi, for their support and guidance. I am likewise grateful to Dr. Jun Tong, Dr. Yanguang Yu, and my research group members Mr. Yuxi Ruan, Ms. Yan Gao, Mr. Wei Han, Ms. Xiaochen He, Ms. Ying Liu, Mr. Weikang Zhao, Mr. Yuanlong Fan, Mr. Lei Lu for their insightful discussion and invaluable help through the tough time.

Finally, I wish to express my sincere appreciation to my family for their great support and love throughout my life. Without their help, it is impossible for me to reach this stage.

Chapter 1

Introduction

1.1 Background

Over the past three decades, wireless communication systems have experienced a tremendous development promoted by the rapid advance of technologies and science. With the evolution of wireless communications, wireless communication systems have been penetrating into people's daily lives. Meanwhile, the number of subscribers in mobile communication systems has seen an extraordinary growth and mobile services have been expanded to a variety of services such as voice call, text and picture messaging, video conference, Internet access, etc.

The intention of future mobile communication systems is to provide reliable communications even under high mobility environments. A relevant practical application is the global demand for wireless communications in high speed railways, where the speed can reach up to 380 km/h for commercial use [1]. Compared to the general scenarios in mobile communication systems, one of the challenging issues in high mobility wireless communication systems is the large Doppler spread. For example, assume that the carrier frequency is f_c = 1.8 GHz and the velocity of a mobile user is v = 300 km/h. Thus, the maximum

Doppler frequency is f_d = 500 Hz. Due to multipath propagation and Doppler spread, transmitted signals under high mobility scenarios will experience fading and distortion, which may lead to high bit error rate and may be a concern for the reliability and effectiveness of mobile communication systems.

The motion of a mobile terminal causes a frequency shift in each multipath component of the transmitted signal, which is referred as Doppler shift. Doppler spread is the spectral broadening caused by the time rate of the change of the wireless channel [2]. As the fading rate of the wireless channel depends on Doppler spread, the knowledge of Doppler spread can be used to compensate and improve communication performance. Since the transmitted signal under high mobility environments will inevitably experience serious deterioration and cause communication performance loss at the receiver side, it is imperative to design efficient algorithms for estimating Doppler spread in order to compensate communication performance.

As Doppler spread is proportional to the velocity of the mobile terminal and it is a significant parameter of the wireless channel, a large number of mobile communication applications can benefit from the accurate estimate of Doppler spread. Adaptive transmission techniques can utilise Doppler spread to reduce complexity or improve performance at the receiver [3]. Some channel estimation techniques can take advantage of the mobile speed to optimise the channel tracker step size [4]. Variable coding, interleaving length adjustment and updating power control algorithm can also benefit from Doppler spread in order to control the transmitter or receiver adaptively for different mobile speeds and reduce reception delay [5, 6]. The knowledge of user's speed can be used in hierarchical cellular

systems for dynamic channel allocation systems [7]. Furthermore, Doppler spread can be used for reducing unnecessary handoffs [8, 9].

1.2 Research Motivations and Objectives

Since the knowledge of Doppler spread is beneficial to these wireless communication applications, an accurate estimate of Doppler spread is indispensable for mobile communication systems. A number of approaches have been developed for Doppler spread estimation. The maximum likelihood (ML) based approach achieves optimal performance, but the complexity is quite high, which can be a concern for practical implementation. The level crossing rate (LCR) based approaches exploit the relationship between the fading rate and the maximum Doppler frequency, which have low complexity, but they need a large number of received samples to guarantee the observation of sufficient level crossings. The covariance based approaches extract the Doppler spread from the autocorrelation function of the wireless channel at different time lags or from the autocovariance of the received signal. The covariance based approaches are more efficient than the LCR based approaches, but the performance degrades when the number of the received samples is relatively small. As the Doppler spread information can be used to characterise the time variation of the fading channels, it can be employed to improve channel estimation performance. Many existing Doppler spread estimation approaches are based on the estimates of channel coefficients and they assume that channel estimates are available at the receiver. Only a few researches concern joint Doppler spread and channel estimation. In [10], an expectation-maximization (EM) based approach was proposed by using a Taylor

series expansion based channel model. However, the complexity of this approach can be a concern. Alternatively, based on an autoregressive (AR) model for the fading channel, an EM based joint channel and AR model coefficients estimation scheme was proposed in [11], where the Doppler spread can be extracted from the estimated AR coefficients. The complexity per iteration of this approach is much lower than that in [10], but the convergence speed may be a concern.

The issues of high complexity and biased estimates in low or high Doppler frequency range exist in some Doppler spread estimation approaches. The objective of this thesis is to design an efficient Doppler spread estimation algorithm with low complexity and good performance over a wide range of maximum Doppler frequency. Due to the mutual dependence of Doppler spread estimation and channel estimation, we aim to jointly estimate Doppler spread and channel coefficients to achieve better performance.

1.3 Research Contributions

The contributions of this thesis are summarised as follows:

In Chapter 3, we proposed a new approach to joint Doppler spread and channel estimation for Rayleigh fading channels through an iterative process between a Doppler spread estimator and a channel estimator. Based on the channel autocorrelation function (ACF), we devise a Doppler spread estimator with an ACF lag selection mechanism which is vital to maximise the Doppler spread performance. Based on a Forney-style factor graph (FFG) representation of the fading channel described by a first order AR (AR(1)) model, we propose a Gaussian message passing (GMP) based channel estimator with optimized AR(1) model coefficients

using the Doppler spread estimate. Compared to the existing joint Doppler spread and channel estimation approaches, the proposed approach achieves similar or better performance with lower complexity.

In Chapter 4, we proposed a low-complexity EM based time-varying channel estimation approach using GMP. By characterising the fading channel with an AR(1) model and representing the fading channel with an FFG, we devise an EM-GMP based approach to jointly estimate the channel coefficients and AR(1) model coefficients. The Doppler spread can be extracted from the estimated AR(1) model coefficients. Compared to the conventional EM algorithm, the proposed EM approach has similar complexity per iteration, but it has a much faster convergence rate.

1.4 Thesis Organisation

The thesis is organised as follows

- Chapter 1 gives an introduction to the thesis background, shows the objectives and highlights the research contributions.
- Chapter 2 first discusses the properties of fading channels, where multipath propagation, Doppler spread, fading channel classification and Clarke fading channel model are presented. Then, it gives a review of existing Doppler spread estimation approaches including ML method, convariance methods, and joint Doppler spread and channel estimation methods. Analyses of theses methods in terms of performance and complexity are provided.
- Chapter 3 first introduces factor graphs and GMP techniques, and then

proposes a new joint Doppler spread and channel estimation approach, where the Doppler spread estimator is based on the ACF of channel estimates with an ACF lag selection mechanism to maximise the Doppler spread performance, and the channel estimator is based on GMP techniques with the optimisation of AR(1) model coefficients using the estimated Doppler spread.

- Chapter 4 first introduces the EM algorithm as message passing, and then with the FFG representation of the fading channel described by an AR(1) model, proposes an EM based joint channel and AR model coefficients estimation approach using GMP techniques.

- Chapter 5 concludes this research and addresses the possible directions for future work.

1.5 Publications

1. Zichen Wang, Yuxi Ruan, Qinghua Guo, Sheng Tong, Jun Tong and Jiangtao Xi, "Low-complexity iterative Doppler spread and channel estimation over Rayleigh fading channels," Submitted to *2015 IEEE/CIC International Conference on Communications in China Signal Processing for Communications Symposium*.

2. Zichen Wang, Qinghua Guo, *et al*, "Low-complexity joint channel and Doppler spread estimation over time-varying frequency selective fading channels," in preparation.

Chapter 2

Literature Review

2.1 Introduction

In this Chapter, we aim to present a comprehensive review of fading channel properties and existing Doppler spread estimation approaches. Doppler spread is inherent to mobile communication systems as it is caused by the relative motion between transmitters and receivers [12]. The environment of mobile communication systems is described by a multipath time-varying fading channel, and it is well known that the knowledge of Doppler spread provides the fading rate of the mobile channel as well as the velocity of the mobile user. Doppler spread information can be utilised for improving performance or reducing complexity in adaptive transmission techniques, channel estimation to optimise channel tracker step size, adjusting interleaving length in order to reduce reception delay, power control, variable coding, reducing unnecessary handoffs and channel allocation in cellular systems [3–6, 8, 13]. With the wide applications, an accurate estimate of the Doppler spread is indispensable to mobile communication systems in order to guarantee effectiveness and efficiency.

The rest of this Chapter is organised as follows. Firstly, we give an intro-

duction of radio wave propagation. Then, we discuss the large-scale effects and small-scale effects which include multipath and Doppler spread. Next, we discuss fading channel classification and introduce Rayleigh fading Distribution as well as the well known Clarke model. After that, we review some Doppler spread estimation approaches. In addition, the linear minimum mean square error (LMMSE) method for channel estimation is included. Last, we conclude this Chapter and come up with an idea of joint Doppler spread and channel estimation to achieve better performance.

2.2 Radio Wave Propagation

In wireless communication systems, a wireless channel refers to a logical connection over a multiplexed medium such as a radio wave, which is used as a physical medium to transmit signals from a transmitter to a receiver in space. Different from wired channels, e.g., open wires which are stationary and predictable, wireless channels are extremely random and present severe impairments for wireless communications systems. These impairments include distortions, noises, interferences and other impediments which are time-varying and unpredictable as a result of terminal movement [14]. The received signal suffers from path loss and fading during propagation processes. In general, mobile radio propagation has large-scale effects and small-scale effects on the received signal. The large-scale propagation effects refer to variations in the received power due to path loss and shadowing, which are over relatively long distances and vary slowly with time. The small-scale propagation effects refer to rapid fluctuations of the received signal power due to multipath and Doppler spread, which are over relatively short

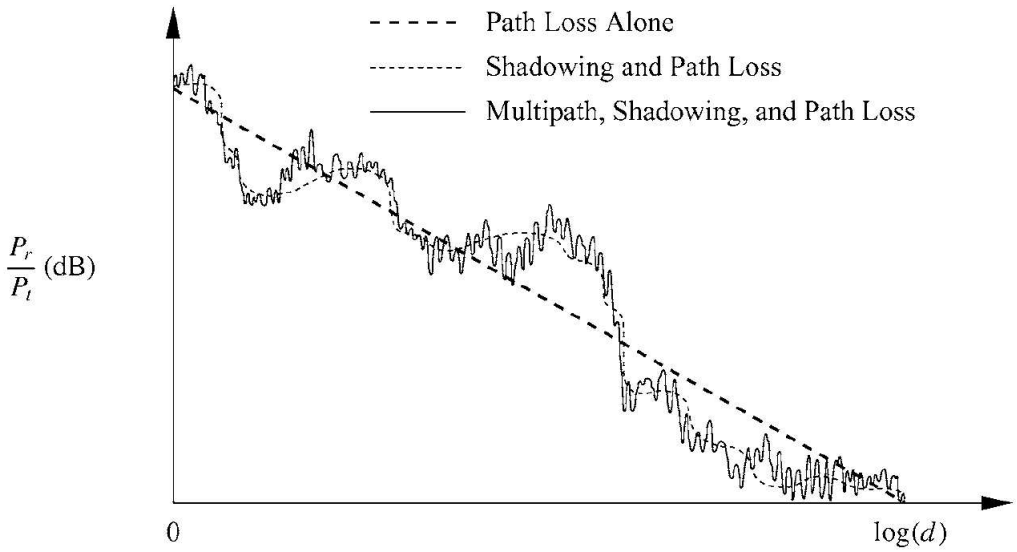

Figure 2.1: Path loss, shadowing and multipath versus distance.

distances. Fig. 2.1 shows the ratio of the received-to-transmit power versus log distances for the combined effects of path loss, shadowing and multipath [14].

2.2.1 Large-scale Effects

Large-scale propagation effects are used to describe variations in the received signal power due to complex terrains in suburbs as well as the density and height of buildings in urban areas. Large-scale effects can be characterised by path loss and shadowing. Path loss is due to power dissipation of the transmitted signal reflected by objects over long distances. Shadowing is caused by large objects, such as mountains and buildings, which attenuates the signal power through reflection, diffraction and scattering [14]. Large-scale effects are significant for predicting the coverage and availability of services [15].

2.2.2 Small-scale Effects

Small-scale effects are used to characterize the rapid fluctuations of the amplitudes, phases and delays of a transmitted signal over a short period of time or a

short distance [2]. Two significant effects of small-scale fading are time dispersion caused by multipath propagation and frequency dispersion caused by Doppler spread [15].

2.2.2.1 Multipath

The propagation path of a transmitted signal between a transmitter and a receiver can vary from a direct line (known as the line-of-sight (LOS)) to one that is refracted by large objects such as buildings and mountains [2], as shown in Fig. 2.2. Generally, there are more than one propagation paths from the transmitter to the receiver due to the terrain and surrounding objects of the receiver. As a result of reflection, diffraction and scattering, multiple versions of the transmitted signal arrive at the receiver with different delays. These radio waves, called multipath waves, sum together to produce a composite received signal. The signal received by the mobile terminal may consist of a large number of plane waves which have randomly distributed amplitudes, phases and angles of arrival. These received signals with different delays sum in a constructive or destructive fashion and cause the composite received signal to fade, distortion or both. [2]. Due to the constructive and destructive effects of multiple received signals combining at the receiver, a mobile terminal with high velocity can suffer several fades in a short time.

Wireless channels introduce delay spread into the received signal, which means the received signal has a longer duration than that of the transmitted signal as a result of different delays of multipath propagation [15]. To be specific, it is a measure of the time difference between the first significant received

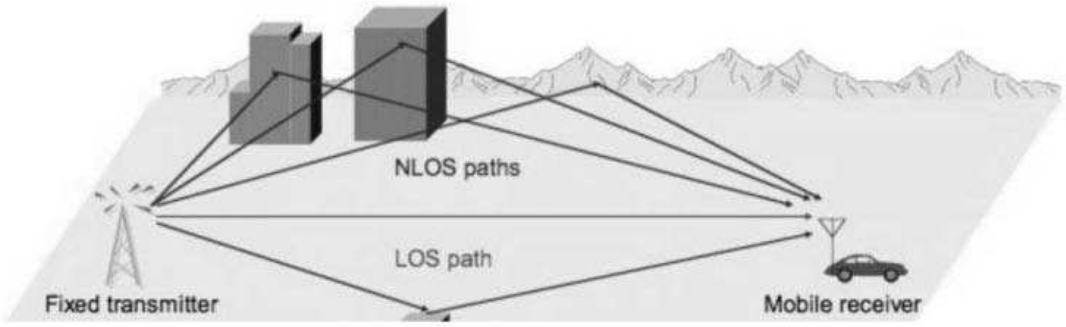

Figure 2.2: Multipath signal propagation.

multipath component (usually the LOS component) and the last received multipath component. The multipath delay spread causes frequency selective fading and inter-symbol interference (ISI). The frequency selective fading means that the channel impulse response has a multipath delay spread and the channel does not affect all frequency components of the signal equally [15]. ISI is referred to as the interference between consecutive symbols, which means that the energy can spread from one symbol to the following symbol and certain frequency components in the received signal spectrum have greater gains than others. Frequency selective fading and ISI lead to signal distortions and performance degradations in wireless communication systems.

The time dispersive nature of the channel can be described by the delay spread and coherence bandwidth. The delay spread is usually quantified by root mean square (RMS) delay spread σ_τ. It is a natural phenomenon caused by reflections and scatterings in wireless channels. The inverse of the RMS delay spread is called coherence bandwidth B_c which is a statistical measure of the frequency range over which a channel affects the signal spectrum in the same way causing a approximately constant attenuation and linear change in phase [2].

2.2.2.2 Doppler Spread

The motion of a mobile terminal leads to a variation in the received signal. Due to the motion, each multipath component experiences a frequency shift, called Doppler shift. The rate of variation of the received signal depends on the velocity of the mobile terminal. Let us assume that a mobile user is moving at a constant velocity v from point X to point Y. Meanwhile it receives signals from a base station S, as shown in Fig. 2.3. The phase change in the received signal is given by

$$\Delta\phi = \frac{2\pi v \Delta t}{\lambda} \cos\theta \tag{2.1}$$

where Δt is the time required for the user to travel from X to Y, $\lambda = c/f_c$ is the radio wave length, c is the speed of light, f_c is the carrier frequency and θ is the angle of arrival. It is assumed that θ remains the same at X and Y as the base station is far away. The Doppler shift can be represented as

$$f = \frac{1}{2\pi} \cdot \frac{\Delta\phi}{\Delta t} = \frac{v f_c}{c} \cos\theta. \tag{2.2}$$

The maximum Doppler frequency can be expressed as

$$f_d = \frac{v f_c}{c}. \tag{2.3}$$

Since the mobile velocity is related to the maximum Doppler frequency, we can obtain the mobile velocity through estimating the maximum Doppler frequency of the fading channel.

Due to the multipath propagation, each multipath wave arrives at the receiver from different directions causing Doppler spread of the received signal, which has a broadening effect on the signal bandwidth. The mobile channel introduces

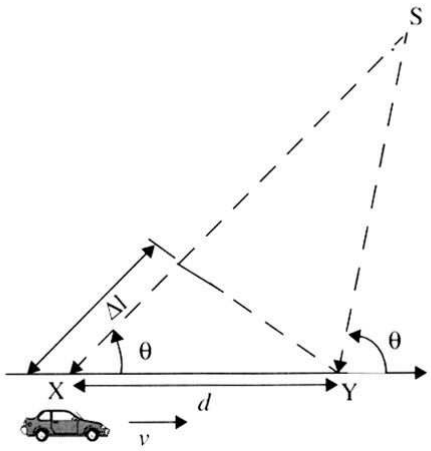

Figure 2.3: Illustration of Doppler shift.

Doppler spread into the received signal, which means that the received signal has a larger bandwidth than that of the transmitted signal as a result of different Doppler shifts experienced by the multipath components. The Doppler spread B_D is a measure of the spectral broadening caused by the time rate of the change of the mobile radio channel [2].

Doppler spread and coherence time are used to characterise the time-varying nature of the mobile channel. The time domain equivalence of Doppler spread is called coherence time T_C which is inversely proportional to Doppler spread. The coherence time is a statistical measure of the time duration over which the channel impulse response is invariant [2].

2.3 Fading Channel Classification

Different transmitted signals will undergo different types of fading, which depends on the relationship between the nature of the transmitted signal and the mobile radio channel. The fading channels can be classified into two categories in terms of time dispersion (caused by multipath) and frequency dispersion (caused

by Doppler spread). The time dispersion and frequency dispersion mechanisms in a mobile radio channel lead to four possible distinct effects, which are depending on the feature of the mobile channel, the transmitted signal and the velocity. The multipath delay spread leads to time dispersion and frequency selective fading, while Doppler spread leads to frequency dispersion and time selective fading [2].

2.3.1 Flat and Frequency Selective Fading

The time dispersion causes the transmitted signal to experience either flat or frequency selective fading [2, 15]. Flat fading occurs when the channel coherence bandwidth B_C is much greater than the transmitted signal bandwidth B_S. In the time domain, this means that the channel RMS delay spread σ_τ is much smaller than the signal symbol period T_S.

$$B_C \gg B_S \tag{2.4}$$

$$\sigma_\tau \ll T_S. \tag{2.5}$$

In flat fading, the amplitude of the received signal varies in gain, but all frequency components of the signal experience the same magnitude of fading and the spectrum of the transmitted signal is not distorted.

Frequency selective fading occurs when the channel coherence bandwidth B_C is smaller than the transmitted signal bandwidth B_S. In the time domain, this means that the channel RMS delay spread σ_τ is larger than the signal symbol period T_S.

$$B_C < B_S \tag{2.6}$$

$$\sigma_\tau > T_S. \tag{2.7}$$

Viewed in the frequency domain, different components of the signal may be affected differently by the channel and the spectrum of the transmitted signal will be distorted at the receiver.

2.3.2 Slow and Fast Fading

A channel can be classified either as a slow fading channel or a fast fading channel depending on how rapidly the transmitted signal changes compared to the rate of change of the channel. In a slow fading channel, the rate of change of the channel is much slower than that of the transmitted signal, which means that the channel coherence time T_C is much larger than the symbol period T_S. In the frequency domain, the Doppler spread B_D is much less than the transmitted signal bandwidth.

$$T_C \gg T_S \tag{2.8}$$

$$B_D \ll B_S. \tag{2.9}$$

In a slow fading channel, the effects of Doppler spread may be negligible.

The fast fading channel causes frequency dispersion due to the Doppler spread, which leads to signal distortion. In a fast fading channel, the channel impulse response changes significantly when the mobile terminal moves fast. The channel coherence time is smaller than the symbol period of the transmitted signal. In frequency domain, the Doppler spread is larger than the bandwidth of the transmitted signal.

$$T_C < T_S \tag{2.10}$$

$$B_D > B_S. \tag{2.11}$$

2.4 Rayleigh Fading Distribution

Rayleigh fading model is a statistical model for characterising the propagation effect of a radio signal. According to the central limit theorem, the complex received envelope can be treated as a wide-sense stationary (WSS) complex Gaussian process since the composite received signal consists of a large number of multipath components. The received complex envelope can be expressed as,

$$Z(t) = Z_I(t) + jZ_Q(t) \tag{2.12}$$

where $Z_I(t)$ and $Z_Q(t)$ are independent and identically distributed (i.i.d.) Gaussian random variables with zero-mean and variance σ^2. Under these conditions, the amplitude of the received complex envelope can be represented as

$$R(t) = \sqrt{Z_I(t)^2 + Z_Q(t)^2}. \tag{2.13}$$

The amplitude of the received complex envelope has a Rayleigh distribution [2, 8, 15]

$$P_R(x) = \frac{x}{\sigma^2} e^{-\frac{x^2}{2\sigma^2}}. \tag{2.14}$$

The Rayleigh fading model is commonly used in urban areas, where many objects reflect and scatter the signal before it arrives at the receiver. There is no LOS component between the transmitter and the receiver. If there is a LOS component arriving at the receiver in the environment, $Z_I(t)$ and $Z_Q(t)$ are Gaussian random process with means $m_I(t)$ and $m_Q(t)$ respectively. We assume $Z_I(t)$ and $Z_Q(t)$ are i.i.d. with the same variance σ^2, and the received complex envelope has a Rician distribution

$$P_R(x) = \frac{x}{\sigma^2} e^{-\frac{x^2+S^2}{2\sigma^2}} I_0(\frac{Sx}{\sigma^2}) \tag{2.15}$$

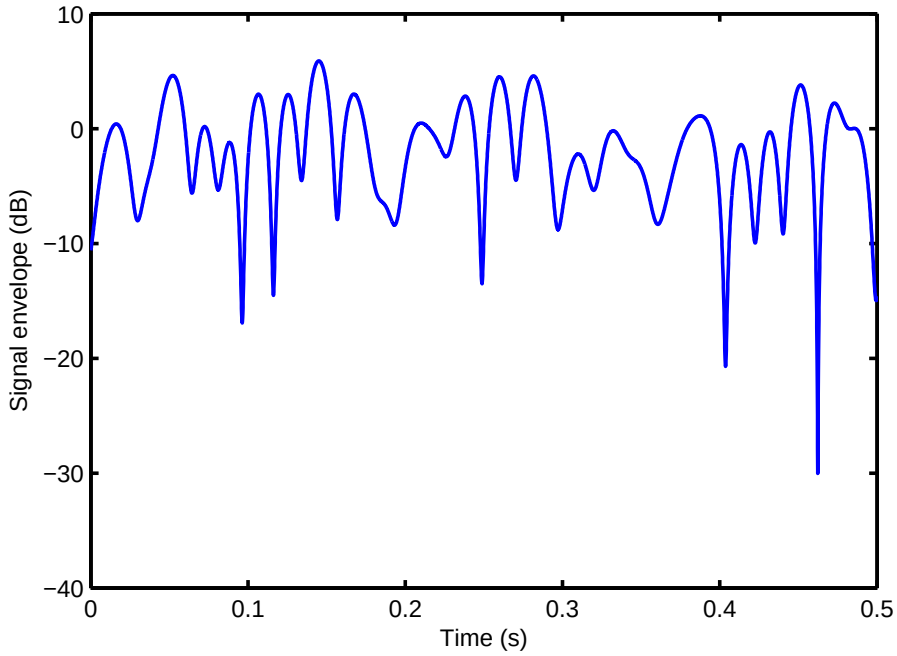

Figure 2.4: Simulated Rayleigh fading envelope with $f_d = 30Hz$.

where $S^2 = m_I^2(t) + m_Q^2(t)$ and I_0 is the zeroth order modified Bessel function of the first kind. In a Rician fading channel, the LOS component is stronger than the other multipath components arriving at the receiver with different phases and delays.

Rayleigh fading is a small-scale propagation effect, which will be superimposed with path loss and shadowing as the signal travels. How rapidly the channel varies depending on the speed of the relative motion between the transmitter and the receiver, and the relative motion causes Doppler shift on each multipath component. Fig. 2.4 and Fig. 2.5 show the signal envelope variation of a simulated Rayleigh fading channel [16] with Doppler spreads of 30 Hz and 100 Hz respectively, which correspond to 18 km/h and 60 km/h at carrier frequency f_c = 1.8 GHz. It can be seen that a mobile terminal moving at a high speed can suffer from several fades in a small period of time.

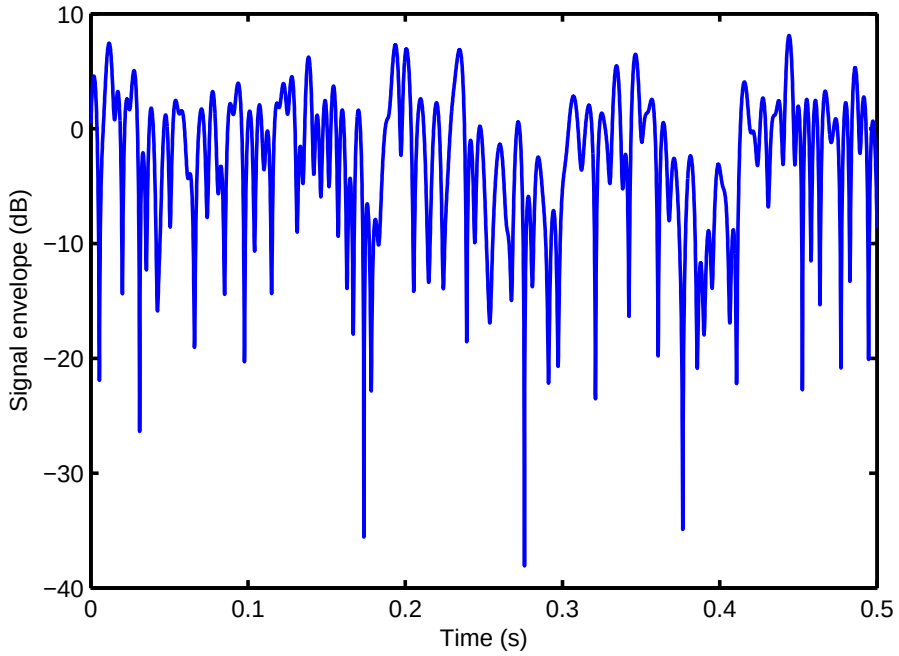

Figure 2.5: Simulated Rayleigh fading envelope with $f_d = 100Hz$.

2.5 Clarke Rayleigh Fading Model

In the last several decades, the well-known mathematical reference model proposed by Clarke [17] and its simplified simulation model proposed by Jakes [12] have been widely used for Rayleigh fading channels. Clarke's model is based on scattering where the statistical properties of the received signal are deduced from scattering [17]. It is assumed that, in the absence of the LOS path, the received signal is comprised of N plane waves from all directions with arbitrary phases, arbitrary angles of arrival and equal average amplitudes. In addition, the distance between a base station and a mobile terminal is sufficiently large, so that the radio propagation environment can be modeled as two-dimensions.

Consider the transmission of the band-pass signal in [8]

$$x(t) = \Re\left[\tilde{x}(t)e^{j2\pi f_c t}\right] \tag{2.16}$$

where $\tilde{x}(t)$ is the complex envelope of the transmitted signal, f_c is the carrier frequency, and $\Re[\cdot]$ denotes the real part of $[\cdot]$. Now consider the mobile terminal in Fig. 2.3. The received noiseless band-pass waveform is [8]

$$r(t) = \Re\left[\sum_{n=1}^{N} C_n e^{j2\pi[(f_c+f_d\cos\theta_n)(t-\tau_n)]}\tilde{x}(t-\tau_n)\right] \tag{2.17}$$

where N is the number of different scattering paths, f_d is the maximum Doppler frequency, C_n, θ_n and τ_n are the amplitude, the incoming angle of arrival and the time delay, respectively. The received complex envelope band-pass signal can be represented as [8]

$$\tilde{r}(t) = \sum_{n=1}^{N} C_n e^{-j\phi_n(t)}\tilde{x}(t-\tau_n), \tag{2.18}$$

where $\phi_n(t) = 2\pi\left[(f_c + f_d\cos\theta_n)\tau_n - f_d\cos\theta_n t\right]$ is the phase associated with the nth path. The complex channel response is given by

$$h(t) = \sum_{n=1}^{N} C_n e^{-j\phi_n(t)}. \tag{2.19}$$

In a flat fading channel, by assuming $\tilde{x} = 1$, the received band-pass signal can be represented as [8]

$$r(t) = h_I(t)\cos 2\pi f_c t - h_Q(t)\sin 2\pi f_c t \tag{2.20}$$

where

$$h_I(t) = \sum_{n=1}^{N} C_n\cos\phi_n(t) \tag{2.21}$$

$$h_Q(t) = \sum_{n=1}^{N} C_n\sin\phi_n(t) \tag{2.22}$$

are the inphase and quadrature part of the received band-pass signal. According to the central limit theorem, $h_I(t)$ and $h_Q(t)$ can be treated as Gaussian random processes as the number of multipath components N is sufficiently large. Under

the assumption that the band-pass process is WSS, the autocorrelation of $r(t)$ is given by

$$\begin{aligned} R_{rr}(\tau) &= E\left[r(t)r(t+\tau)\right] \\ &= R_{h_I h_I}(\tau)\cos 2\pi f_c \tau - R_{h_Q h_I}(\tau)\sin 2\pi f_c \tau \end{aligned} \tag{2.23}$$

where $R_{h_I h_I}(\tau) = R_{h_Q h_Q}(\tau)$ and $R_{h_I h_Q}(\tau) = R_{h_Q h_I}(-\tau)$. It is assumed that $\phi_n(t)$ is uniformly distributed over $[-\pi, \pi]$. It may be assumed that $\phi_n(t)$ is independent, since delay τ_n and the maximum Doppler frequency f_d are independent [8]. Based on these properties, $R_{g_I g_I}(\tau)$ can be obtained as

$$R_{h_I h_I}(\tau) = \frac{\sigma_h^2}{2} E_\theta\left[\cos(2\pi f_d \tau \cos\theta)\right] \tag{2.24}$$

where $\theta = (\theta_1, \theta_2, \ldots, \theta_N)$ is the nth multipath angle of arrival, and σ_h^2 is the total received envelope power. Note that the power in the band-pass waveform $r(t)$ is $\sigma_h^2/2$. The crosscorrelation $R_{h_I h_Q}(\tau)$ is

$$R_{h_I h_Q}(\tau) = \frac{\sigma_h^2}{2} E_\theta\left[\sin(2\pi f_d \tau \cos\theta)\right]. \tag{2.25}$$

In order to evaluate the expectations in (2.24) and (2.25), the distribution of the incident power on the receiver antenna $p(\theta)$ and the receiver antenna gain $G(\theta)$ as a function of the angel of arrival are required [8]. We have $p(\theta) = 1/(2\pi)$, $\theta \in [-\pi, \pi]$ and $G(\theta) = 1$, since we assume that the plane waves arrive at the mobile receiver from all directions with equal probability and 2-D isotropic scattering. Thus, the autocorrelation of $R_{h_I h_I}(\tau)$ is given by [8]

$$\begin{aligned} R_{h_I h_I}(\tau) &= \frac{\sigma_h^2}{2}\int_{-\pi}^{\pi} \cos(2\pi f_d \tau \cos\theta) p(\theta) G(\theta) \mathrm{d}\theta \\ &= \frac{\sigma_h^2}{2} J_0(2\pi f_d \tau) \end{aligned} \tag{2.26}$$

where $J_0(\cdot)$ is the zeroth order Bessel function of the first kind. The crosscorrelation

of $R_{h_I h_Q}(\tau)$ becomes

$$\begin{aligned} R_{h_I h_Q}(\tau) &= \frac{\sigma_h^2}{2} \int_{-\pi}^{\pi} \sin(2\pi f_d \tau \cos\theta) p(\theta) G(\theta) \mathrm{d}\theta \\ &= 0. \end{aligned} \tag{2.27}$$

The autocorrelation of $h(t) = h_I(t) + jh_Q(t)$ is given by

$$\begin{aligned} R_{hh}(\tau) &= E\left[h(t)h^*(t+\tau)\right] \\ &= \sigma_h^2 J_0(2\pi f_d \tau). \end{aligned} \tag{2.28}$$

The power density spectrum of $h(t)$ is the Fourier transform of the autocorrelation of $R_{hh}(\tau)$, which can be shown as

$$\begin{aligned} S(f) &= \mathcal{F}\left[R_{hh}(\tau)\right] \\ &= \begin{cases} \frac{\sigma_h^2}{\pi f_d \sqrt{1-\left(f-f_d\right)^2}}, & \left|f\right| \le f_d \\ 0, & \text{otherwise.} \end{cases} \end{aligned} \tag{2.29}$$

The normalized autocorrelation function of a flat Rayleigh fading channel with $f_d = 200Hz$ and the Doppler spectrum are shown in Fig. 2.6 and Fig. 2.7, respectively.

2.6 Review of Doppler Spread Estimation Approaches

Doppler spread estimation has been extensively studied and a number of methods have been proposed over the past several decades. Generally, Doppler spread estimates are usually obtained from the channel coefficients or received signals. There are four categories of Doppler spread estimation schemes in the literatures: level-crossing rate (LCR) based methods [8, 18–22], power spectrum density (PSD) based methods [23–26], covariance based methods [4–6, 9, 13, 27–38] and maximum likelihood (ML) based methods [3, 39–44].

LCR refers to how often an envelope crosses a specified level and is defined as the rate of the envelope crossing the specified level with positive (or negative)

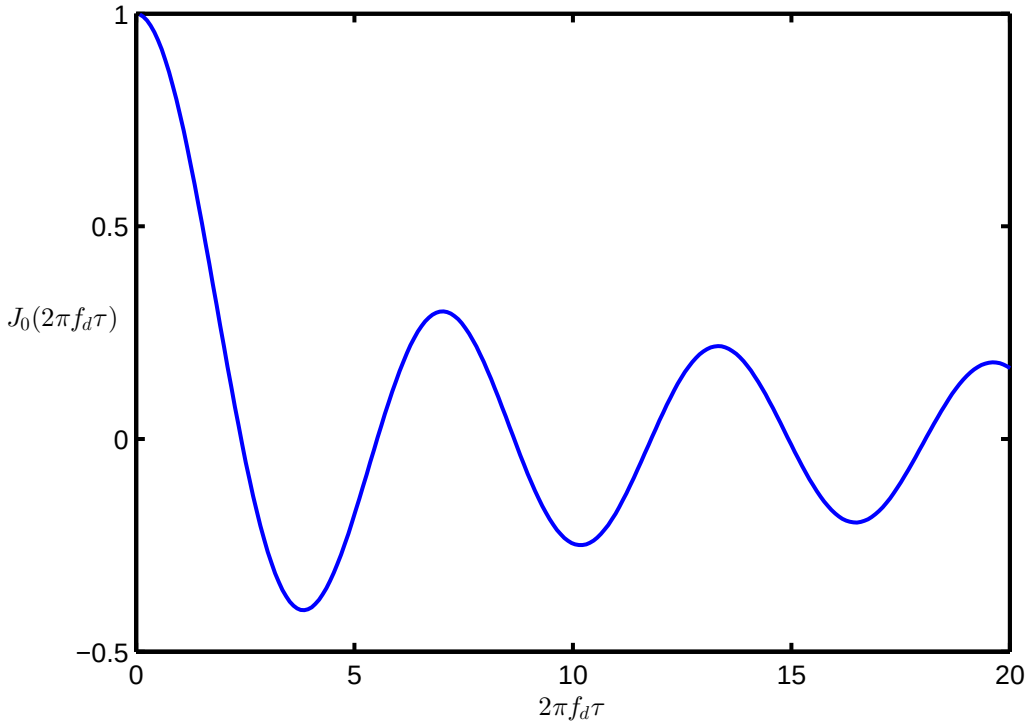

Figure 2.6: Normalized autocorrelation function of a flat Rayleigh fading channel with $f_d = 200Hz$.

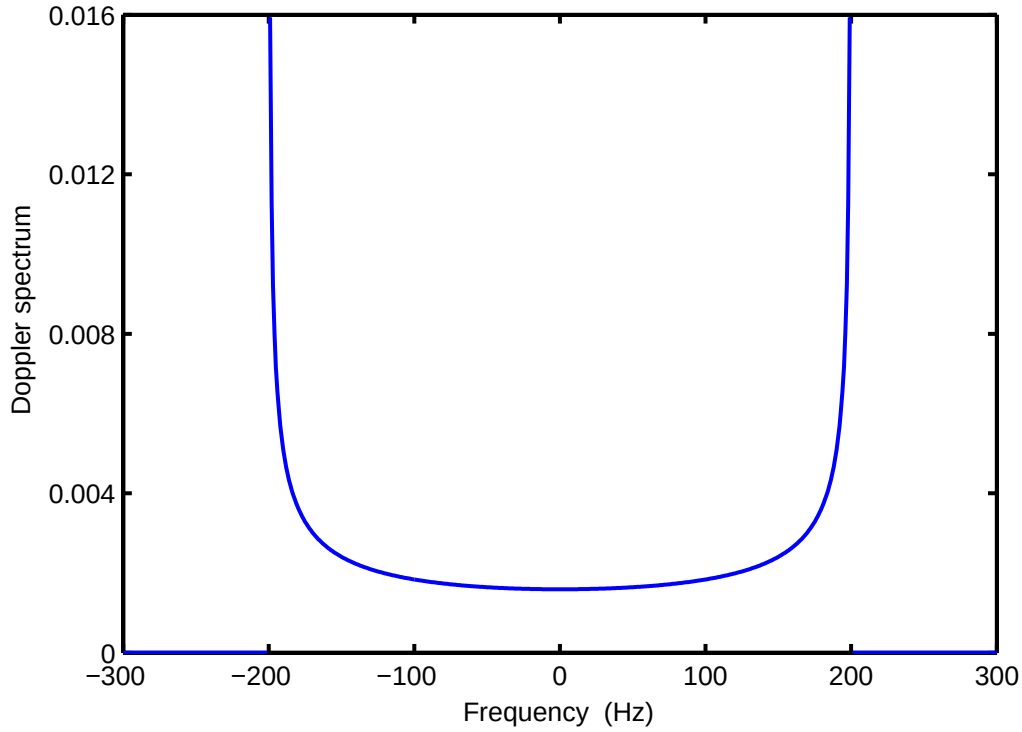

Figure 2.7: Doppler spectrum with $f_d = 200Hz$.

slope. The LCR based estimators depend on the number of the envelope level crossings which is proportional to the maximum Doppler frequency. Theses approaches exploit the relationship between the fading rate and the Doppler spread, which have low complexity, but a large number of received samples are needed to guarantee the observation of sufficient level crossings for low Doppler frequencies.

Based on some assumptions, the PSD based approaches extract the Doppler spread by using some particular features from the Doppler spectrum. The performance of the PSD based estimators degrades drastically when the number of the received samples is relatively small. The PSD schemes suffer from channel estimation error since the spectrum is the Fourier transform of the channel autocorrelation function.

The covariance based approaches exploit the Doppler spread from the channel autocorrelation function (ACF) at different time lags or from the auto-covariance of the received signal, which are generally more efficient than the LCR based methods [6, 32, 36, 44], but the performance degrades when the number of the received signal is relatively small, especially in low Doppler spread range.

The ML based approaches which utilise the channel coefficients directly, are known to be more accurate than the other approaches, but the complexity cost is much higher than other methods, which can be a concern for practical implementation.

Most of these approaches [3, 5, 13, 24, 29, 30, 32, 33, 36, 42, 44] assume that the channel estimates are available before estimating Doppler spread. As the Doppler spread information can be used to characterise the time variation of the

fading channel, it can be employed to improve the channel estimation performance. On the other hand, some channel estimation techniques simply assume that the Doppler information is known at the receiver [45–48]. The mutual dependence of Doppler spread estimation and channel estimation motivated joint Doppler spread and channel estimation to achieve better performance. Only a few researches investigated joint Doppler spread and channel estimation [10, 11].

As in [3, 10, 13, 33, 49], we discuss the reviewed approaches with flat Rayleigh fading channels. The received baseband signal at time instance k can be expressed as

$$r_k = h_k x_k + n_k, \quad k = 0, 1, \cdots, K-1 \tag{2.30}$$

where h_k is complex Gaussian distributed channel coefficient with channel power σ_h^2, x_k is the transmitted symbol and n_k is a complex additive white Gaussian noise (AWGN) with zero mean and variance σ_n^2.

2.6.1 Covariance Based Doppler Spread Estimation

In this subsection, we review two covariance based estimators, the sample covariance (SC) based approach [13] and the zero crossing point (ZCP) based approach [30], respectively. The SC approach is based on the second spectral moment of the in-phase or quadrature-phase (I/Q) components. The ZCP approach is based on finding the ZCP of the channel ACF.

2.6.1.1 Sample Correlation Approach

Based on the sample correlations of the I/Q components and by assuming the channel coefficients are available, a novel Doppler spread estimator was proposed in [13]. This approach exploits the relationship between the Doppler spread

Table 2.1: Steps for the SC Based Doppler Spread Estimation Approach

1. Find the correlation estimates $\left\{\hat{R}_h(lT_s)\right\}_{l=0}^{L}$ by sample averaging.
2. Find $\hat{a}_k = \arg\min_{a_k} \sum_{l=0}^{L} \left|\hat{R}_h(lT_s) - \sum_{k=0,2}^{2} a_k l^k\right|^2$, $k = 0, 2$.
3. Obtain $\hat{R}_h^{(n)}(0) = n!\hat{a}_n / T_s^n, \quad n = 0, 2.$
4. Substitute $\hat{R}_h^{(n)}(0), \quad n = 0, 2$, in (2.31).

and the second spectral moment for Doppler spread estimation. The maximum Doppler frequency can be expressed as [13]

$$f_d = \sqrt{\frac{-2R_h''(0)}{R_h(0)}} / (2\pi T_s) \tag{2.31}$$

where $R_h(\tau) = \sigma_h^2 J_0(2\pi f_d \tau)$, $R_h''(0)$ is the curvature of $R_h(\tau)$ at zero and T_s is the sampling time. In order to estimate $R_h(0)$ and $R_h''(0)$, a scheme by fitting a parabola of the Taylor's series to the L points of sample correlations $\left\{\hat{R}_h(lT_s)\right\}_{l=0}^{L}$ is proposed. It also assumes that the sampling time T_s is sufficiently small to insure $LT_s \ll 1$, which is satisfied for the channel estimators of narrow band time division multiple access systems. The steps for the SC based Doppler spread estimation approach is summarised in Table 2.1.

The SC method has a low computational cost due to the use of a second order polynomial, but the performance degrades in high Doppler frequency range [49]. Higher order polynomial can enhance the estimation performance, but the complexity also increases. The value of L is important, as it refers to how many times the algorithm needs to calculate the sample correlations and it is related to the accuracy of fitting the sample correlations, where a larger L can achieve better performance at the cost of higher complexity.

2.6.1.2 Zero Crossing Point Approach

The ZCP method aims to detect the first zero point of the channel ACF, where the channel coefficients are assumed to be available by some channel estimation techniques. Since the normalised channel ACF $R_h(lT_s) = J_0(2\pi f_d l T_s)$, the first zero crossing point can be given by

$$R_h(lT_s) = J_0(2\pi f_d l T_s) = 0 \tag{2.32}$$

where l is the time lag. We can rewrite (2.32) and the time lag l is given by

$$l = \frac{J_0^{-1}(0)}{2\pi f_d T_s} \approx \frac{2.4048}{2\pi f_d T_s}. \tag{2.33}$$

The task is to select l. After the lag l corresponding to the ZCP is determined, the maximum Doppler frequency can be estimated by

$$f_d = \frac{2.4048}{2\pi l T_s}. \tag{2.34}$$

Linear or cubic spline interpolation technique can be used to find the time lag, where cubic spline interpolation is more accurate than linear interpolation, but the complexity of cubic spline interpolation is higher than that of linear interpolation. The steps for ZCP based Doppler spread estimation approach is summarised in Table 2.2.

The first zero point may not be detected in low Doppler frequency range due to a small number of received samples. Hence, the ZCP based Doppler spread estimator requires a large number of received samples to guarantee a possible ZCP. As f_d is inversely proportional to l, it needs many calculations of the channel ACF to obtain the first zero point. Therefore, the computational cost is relatively high. In [30], by determining the sign of the channel autocorrelation function, a

Table 2.2: Steps for the ZCP Based Doppler Spread Estimation Approach

1. Calculate the channel ACFs where the value of the time lag depends on the length of transmitted symbol.
2. Find the first minimum positive value and the first maximum negative value from the calculated ACF.
3. Exploit the interpolation technique between the two selected points to find the time lag l which corresponds to the fist zero point.
4. Estimate the maximum Doppler frequency by substituting the time lag l into (2.34).

hybrid Doppler spread estimator which separates the Doppler spread into slow mode and fast mode was proposed. If the minimum value of $R_h(lT_s)$ is greater than zero, the Doppler spread is in slow mode, otherwise it is in fast mode. The SC approach is used for the slow mode and the ZCP approach is used for the fast mode. It is noted that in order to achieve better performance, a fourth order polynomial fit to $\left\{\hat{R}_h(lT_s)\right\}_{l=0}^{L}$ is employed in [30] instead of the second order polynomial in [13]. The complexity of the approach in [30] is higher than that of the SC approach in [13].

2.6.2 Maximum Likelihood Based Doppler Spread Estimation

The ML based Doppler spread estimation is known as the optimal approach by taking advantage of the correlation property of channel coefficients. Assume that a vector form estimate of channel coefficients $\hat{\mathbf{h}}$ is available by any channel estimation algorithm. The probability density function (PDF) of $\hat{\mathbf{h}}$ can be represented as

$$p(\hat{\mathbf{h}}; f_d) = \frac{1}{\pi^K \det\left(\mathbf{C}_{\hat{\mathbf{h}}\hat{\mathbf{h}}}(f_d)\right)} \mathrm{e}(-\hat{\mathbf{h}}^H \mathbf{C}^{-1}_{\hat{\mathbf{h}}\hat{\mathbf{h}}}(f_d)\hat{\mathbf{h}}) \tag{2.35}$$

where $\mathbf{C}_{\hat{\mathbf{h}}\hat{\mathbf{h}}}(f_d)$ is the covariance matrix of the estimated channel coefficients, and it can be expressed as

$$\mathbf{C}_{\hat{\mathbf{h}}\hat{\mathbf{h}}}(f_d) = \mathbf{C}_{\mathbf{hh}}(f_d) + \sigma_n^2\mathbf{I} \tag{2.36}$$

where $\mathbf{C}_{\mathbf{hh}}(f_d)$ is the covariance matrix of the true channel coefficients, σ_n^2 is the noise variance and $\mathbf{I}$ is a $K \times K$ identity matrix. The log-likelihood function (LLF) for a maximum Doppler frequency is given by [3]

$$L(\hat{\mathbf{h}}; f_d) = \log\left[\det\left(\mathbf{C}_{\hat{\mathbf{h}}\hat{\mathbf{h}}}(f_d)\right)\right] + \hat{\mathbf{h}}^H\mathbf{C}_{\hat{\mathbf{h}}\hat{\mathbf{h}}}^{-1}(f_d)\hat{\mathbf{h}} \tag{2.37}$$

To minimise the LLF by searching the unknown maximum Doppler frequency, it requires the inverse operation of a $K \times K$ size covariance matrix $\mathbf{C}_{\hat{\mathbf{h}}\hat{\mathbf{h}}}(f_d)$ and the computation of its determinant. The computational complexity is $\mathcal{O}(K^3)$ which can be a concern for practical implementation. In [3], based on matching the channel ACF, a suboptimal estimator which does not require the matrix inversion and signal-to-noise ratio (SNR), is proposed at the cost of performance degradation, where the computational complexity is $\mathcal{O}(K^2)$.

To further reduce the complexity, based on a N-th order Taylor series expansion of the actual channel ACF, an approximate ML Doppler spread estimator was proposed in [42] for low to medium user velocity with a relatively small number of observations. Although the complexity reduces from $\mathcal{O}(K^3)$ to $\mathcal{O}(N^3)$ ($N \ll K$), it still has to calculate some multiplications of predefined matrices, where the complexity remains high. In addition, the approximate ML estimator in [42] suffers from numerical instabilities of searching the optimal Doppler frequency due to the inverse operation of the approximate covariance matrix. In addition, the performance of approximate ML Doppler spread estimator degrades in high

Doppler spread range.

2.6.3 Joint Doppler Spread and channel Estimation

2.6.3.1 EM Based Approach with Taylor Series Expansion Channel Model

Recently, a joint Doppler spread and channel estimation approach was proposed for flat Rayleigh fading channels [10]. By using a Taylor series expansion to approximate the fading channel, it employs the expectation-maximization (EM) algorithm to attain the ML joint Doppler spread and channel estimates iteratively.

The continuous-time channel response can be represented as [10]

$$h(t) = \sum_{m=1}^{M} \alpha_m e^{j(2\pi f_d t \cos\theta_m + \phi_m)} \tag{2.38}$$

where M is the number of scattering path, α_m, θ_m and ϕ_m is the amplitude, the angle of income wave and the initial phase of the m-th path, respectively. By using a P-th order Taylor series expansion at $t = 0$ to approximate $h(t)$, the fading channel can be represented as [10]

$$h(t) \approx \sum_{p=0}^{P} (2\pi f_d t)^p \frac{j^p}{p!} \sum_{m=1}^{M} \alpha_m e^{j\phi_m} (\cos\theta_m)^p. \tag{2.39}$$

Based on (2.39), the discrete-time channel vector can be expressed as [10]

$$\begin{aligned} \mathbf{h} &= [h_0, h_1, \cdots, h_{K-1}]^T \\ &= [\mathbf{v}_0, \mathbf{v}_1, \cdots, \mathbf{v}_P] \cdot \mathrm{diag}(\left[f_d^0, f_d^1, \cdots, f_d^P\right]^T) \cdot [\eta_0, \eta_1, \cdots, \eta_P]^T \\ &= \mathbf{V}\mathbf{D}_f\boldsymbol{\eta} \end{aligned} \tag{2.40}$$

where $\mathbf{V}$ is a Vandermonde matrix with column vectors $\mathbf{v}_p = [(2\pi T_s \cdot 0)^p, (2\pi T_s \cdot 1)^p, \cdots, (2\pi T_s(K-1))^p]^T$ for $0 \le p \le P$, $\mathbf{D}_f$ is a diagonal matrix and $\boldsymbol{\eta}$ is corresponding to channel coefficients with $\eta_p = \frac{j^p}{p!} \sum_{m=1}^{M} \alpha_m e^{j\phi_m} (\cos\theta_m)^p$.

For large M, $\boldsymbol{\eta}$ is a complex circular symmetric Gaussian random vector and the PDF is given by [10]

$$p(\boldsymbol{\eta}) = \frac{1}{\pi^{P+1}\det(\mathbf{R}_\eta)} \mathrm{e}^{-\boldsymbol{\eta}^H \mathbf{R}_\eta^{-1} \boldsymbol{\eta}} \tag{2.41}$$

where $\mathbf{R}_\eta$ is the covariance matrix of $\boldsymbol{\eta}$. Assuming isotropic scattering, equally amplitudes for each path and uniformly distributed for the incoming angles, the covariance matrix can be expressed as

$$\left[\mathbf{R}_\eta\right]_{p,l} = \begin{cases} \frac{(-1)^l j^{p+l}}{p!l!} \frac{\sigma_\eta^2}{2^{p+l}} \binom{p+l}{(p+l)/2}, & \text{if } p+l \text{ is even} \\ 0, & \text{if } p+l \text{ is odd} \end{cases} \tag{2.42}$$

Based on f_d and $\boldsymbol{\eta}$, the PDF of the observation $\mathbf{r}$ is given by [10]

$$p(\mathbf{r}|f_d, \boldsymbol{\eta}) = \frac{1}{(\pi\sigma_n^2)^K} \mathrm{e}(-\frac{1}{\sigma_n^2}|\mathbf{r} - \mathbf{V}\mathbf{D}_f\boldsymbol{\eta}|^2). \tag{2.43}$$

Searching for the optimal f_d and $\boldsymbol{\eta}$ to maximise (2.43) is not feasible due to demanding complexity. The authors employ the EM algorithm to jointly estimate Doppler spread and channel coefficients, where f_d is the unknown parameter and $\boldsymbol{\eta}$ is the missing data.

- E-Step: at the i-th iteration, the E-step takes the expectation over the conditional PDF of the missing data $\boldsymbol{\eta}$, $p(\boldsymbol{\eta}|\mathbf{r}, \hat{f}_d^{(i-1)})$. The expected LLF is [10]

$$Q(f_d|\hat{f}_d^{(i-1)}) = \int \log(p(\mathbf{r}, \boldsymbol{\eta}|f_d)) p(\boldsymbol{\eta}|\mathbf{r}, \hat{f}_d^{(i-1)}) \mathrm{d}\boldsymbol{\eta} \tag{2.44}$$

  where

$$p(\boldsymbol{\eta}|\mathbf{r}, \hat{f}_d^{(i-1)}) = \frac{c_1}{\pi^{P+1}\det(\sigma_n^2(\mathbf{G}^{(i)})^{-1})} \mathrm{e}\left\{-\frac{1}{\sigma_n^2}(\boldsymbol{\eta} - \hat{\boldsymbol{\eta}}^{(i)})^H (\mathbf{G}^{(i)})^{-1} (\boldsymbol{\eta} - \hat{\boldsymbol{\eta}}^{(i)})\right\} \tag{2.45}$$

  with

$$\mathbf{G}^{(i)} = \mathbf{D}_f^{(i-1)} \mathbf{V}^T \mathbf{V} \mathbf{D}_f^{(i-1)} + \sigma_n^2 \mathbf{R}_\eta^{-1}. \tag{2.46}$$

Note that c_1 is a constant. Thus,

$$\hat{\boldsymbol{\eta}}^{(i)} = (\mathbf{G}^{(i)})^{-1}\mathbf{D}_f^{(i-1)}\mathbf{V}^T\mathbf{r} \tag{2.47}$$

is used as the estimate of channel coefficients in vector form. Then, the LLF in (2.44) can be rewritten as [10]

$$\begin{aligned} Q(f_d|\hat{f}_d^{(i-1)}) = \frac{c_2}{\sigma_n^2}\Big(&2\Re\{\mathbf{r}^H\mathbf{V}\mathbf{D}_f\hat{\boldsymbol{\eta}}^{(i)}\} \\ &- \mathrm{Tr}\{\mathbf{D}_f\mathbf{V}^T\mathbf{V}\mathbf{D}_f[\sigma_n^2(\mathbf{G}^{(i)})^{-1} + \hat{\boldsymbol{\eta}}^{(i)}(\hat{\boldsymbol{\eta}}^{(i)})^H]\}\Big) + c_3 \end{aligned} \tag{2.48}$$

where c_2 and c_3 are constants.

- M-step: Find the optimal $\hat{f}_d^{(i)}$ that maximises the LLF in (2.48)

$$\hat{f}_d^{(i)} = \arg\max_{f_d} Q(f_d|\hat{f}_d^{(i-1)}). \tag{2.49}$$

After the EM scheme converges in the i^*-th iteration, the joint Doppler spread and channel estimates are given by [10]

$$\hat{f}_d = \hat{f}_d^{(i^*)}, \tag{2.50a}$$

$$\hat{\mathbf{h}} = \mathbf{V}\mathbf{D}_f^{(i^*)}\hat{\boldsymbol{\eta}}^{(i^*)}. \tag{2.50b}$$

Taking the complexity and performance into consideration, the authors choose the SC based Doppler spread estimation approach in [13] as the initial value for the Doppler spread, where the convergence rate relies on the initialised Doppler spread. The computational complexity of the EM approach in [10] is quite high, since it needs several heavy multiplication operations and the inverse operation of matrices $\mathbf{G}$ and $\mathbf{R}_\eta$ in each iteration. In the simulation, the authors set the order $P = 10$ for the Taylor series expansion based channel model. Simulation results show that the EM approach in [10] has a good performance of channel

estimation from low to medium Doppler spread, but the performance degrades in high Doppler spread. Compared to the ML based Doppler spread estimator [3], it yields biased estimates of Doppler spread in low user velocity.

2.6.3.2 EM Based Approach with AR Channel Model

Based on an autoregressive (AR) model for the fading channel, an EM based joint channel and AR model coefficient estimation scheme was proposed in [11], where the Doppler spread can be extracted from the estimated AR model coefficient. Note that a more complex issue is investigated in [11], i.e., both frequency selective channels and carrier frequency offset are considered.

The time-varying Rayleigh fading channel is approximately described by the following first order AR model

$$h_k = ah_{k-1} + w_k. \tag{2.51}$$

where a is a constant, and w_k is a complex Gaussian noise with zero mean and variance g. The unknown parameter is given as $\Theta = \{\theta_1, \theta_2\}$, where $\theta_1 = \{\sigma_n^2\}$ and $\theta_2 = \{a, g\}$. The ML estimation for Θ is expressed as

$$\hat{\Theta} = \arg\max_{\Theta} \int p(\mathbf{r}, \mathbf{h}|\mathbf{x}, \Theta)\mathrm{d}\mathbf{h} \tag{2.52}$$

where $\mathbf{r}, \mathbf{h}$ and $\mathbf{x}$ are size $K \times 1$ vectors form of the received signal, channel coefficients and transmitted signal, respectively. The conditional PDF $p(\mathbf{r}, \mathbf{h}|\mathbf{x}, \Theta)$ is given as [11]

$$\begin{aligned} p(\mathbf{r}, \mathbf{h}|\mathbf{x}, \Theta) =& p(\mathbf{r}|\mathbf{x}, \mathbf{h}, \theta_1)p(\mathbf{h}|\theta_2) \\ \sim& \frac{1}{(\sigma_n^2)^K}\mathrm{e}\left[-\frac{1}{\sigma_n^2}\sum_{k=1}^{K}|r_k - h_k x_k|^2\right] \\ &\cdot \frac{1}{g^K}\mathrm{e}\left[-\frac{1}{g}\sum_{k=1}^{K}|h_k - ah_{k-1}|^2\right]. \end{aligned} \tag{2.53}$$

The ML estimation for unknown parameters leads to demanding complexity cost. The authors pursue the EM approach to derive an iterative pilot-aided ML estimator for the Rayleigh fading model and the AR model coefficient. The missing data is the channel coefficients in vector form $\mathbf{h}$. The objective function of the EM approach at the i-th iteration is given by [11]

$$Q(\Theta|\hat{\Theta}^{(i-1)}) = \mathrm{E}\left[\log p(\mathbf{r}|\mathbf{x},\mathbf{h},\theta_1)|\mathbf{r},\mathbf{x},\hat{\Theta}^{(i-1)}\right] + \mathrm{E}\left[\log p(\mathbf{h}|\theta_2)|\mathbf{r},\mathbf{x},\hat{\Theta}^{(i-1)}\right], \tag{2.54}$$

where

$$\begin{aligned}\mathrm{E}\left[\log p(\mathbf{r}|\mathbf{x},\mathbf{h},\theta_1)|\mathbf{r},\mathbf{x},\hat{\Theta}^{(i-1)}\right] = &- K\log\sigma_n^2 - \frac{1}{\sigma_n^2} \\ &\times \sum_{k=1}^{K}\Big(|r_k|^2 - 2\Re\{r_k^* x_k \mathrm{E}\left[h_k|\mathbf{r},\mathbf{x},\hat{\Theta}^{(i-1)}\right]\} \\ &+ x_k\mathrm{E}\left[h_k h_k^*|\mathbf{r},\mathbf{x},\hat{\Theta}^{(i-1)}\right]x_k^*\Big),\end{aligned} \tag{2.55}$$

and

$$\begin{aligned}\mathrm{E}\left[\log p(\mathbf{h}|\theta_2)|\mathbf{r},\mathbf{x},\hat{\Theta}^{(i-1)}\right] = &- K\log g - \frac{1}{g} \\ &\times \sum_{k=1}^{K}\Big(\mathrm{E}\left[|h_k|^2|\mathbf{r},\mathbf{x},\hat{\Theta}^{(i-1)}\right] \\ &- 2\Re\{a\mathrm{E}\left[h_{k-1}h_k^*|\mathbf{r},\mathbf{x},\hat{\Theta}^{(i-1)}\right]\} \\ &+ a^2\mathrm{E}\left[h_{k-1}h_{k-1}^*|\mathbf{r},\mathbf{x},\hat{\Theta}^{(i-1)}\right]\Big).\end{aligned} \tag{2.56}$$

The EM algorithm is summarised as follows

- E-step: For $k = 0, 1, \cdots, K$ calculate

$$\mathrm{E}\left[h_k|\mathbf{r},\mathbf{x},\hat{\Theta}^{(i-1)}\right] = \hat{h}_{k|K}^{(i)} \tag{2.57a}$$

$$\mathrm{E}\left[h_k h_k^*|\mathbf{r},\mathbf{x},\hat{\Theta}^{(i-1)}\right] = \hat{h}_{k|K}^{(i)}\hat{h}_{k|K}^{(i)^*} + P_{k|K}^{(i)} = \Phi_k^{(i)} \tag{2.57b}$$

$$\mathrm{E}\left[h_{k-1}h_k^*|\mathbf{r},\mathbf{x},\hat{\Theta}^{(i-1)}\right] = \hat{h}_{k-1|K}^{(i)}\hat{h}_{k|K}^{(i)^*} + P_{k-1,k|K}^{(i)} = \Psi_k^{(i)} \tag{2.57c}$$

  where the channel estimate $\hat{h}_k^{(i)}$ and the variances $P_{k|K}^{(i)}$ and $P_{k-1,k|K}^{(i)}$ can be obtained using the Kalman smoothing equations in [50].

- M-step: By maximising the objective function, the unknown parameters are given by [11]

$$\hat{\sigma_n^2}^{(i)} = \frac{1}{K}\sum_{k=1}^{K}\left(|r_k|^2 - 2\Re\{r_k^* x_k \hat{h}_{k|K}^{(i)}\} + x_k \Phi_k^{(i)} x_k^*\right) \tag{2.58a}$$

$$\hat{a}^{(i)} = \frac{\sum_{k=1}^{K}\Psi_k^{(i)}}{\sum_{k=1}^{K}\Phi_{k-1}^{(i)}} \tag{2.58b}$$

$$\hat{g}^{(i)} = \frac{1}{K}\sum_{k=1}^{K}\left(\Phi_k^{(i)} - \hat{a}^{(i)}\Psi_k^{(i)}\right). \tag{2.58c}$$

The initialised value of the AR model coefficients can be obtained by using the received signal. After the EM algorithm converges, the Doppler spread can be extracted from the estimated AR(1) model coefficient, which can be given as [11]

$$\hat{f_d} = \arccos\left(\frac{1+\hat{a}^2 - \frac{1}{\xi}(1-\hat{a})^2}{2\hat{a}}\right)/(2\pi T_s) \tag{2.59}$$

where ξ is an attenuation of the AR spectrum at the estimated frequency with respect to zero frequency, e.g., $\xi = 0.5$ corresponds to the -3 dB bandwidth [11].

The complexity of the EM approach in [11] and the the EM approach in [10] is $O(17K)$ and $O((P+1)^2K)$ per iteration, respectively. The complexity per iteration of the EM approach in [11] is much lower than that in [10]. The performance of the Doppler spread estimation of the EM approach in [11] degrades in low Doppler frequency range.

2.7 LMMSE Channel Estimation

In this section, we give a brief introduction to the application of linear minimum mean square error (LMMSE) approach for channel estimation. The LMMSE channel estimator will not be optimal unless the Doppler spread is known (where

we use the LMMSE channel estimator as a benchmark for channel performance comparison).

Since the model (2.30) is Bayesian linear model, the LMMSE channel estimator can achieve optimal performance under the condition of known Doppler spread. The model (2.30) can be expressed as a matrix form

$$\mathbf{r} = \mathbf{X}\mathbf{h} + \mathbf{n} \tag{2.60}$$

where $\mathbf{r}$ is a $K\times 1$ vector of the received signal, $\mathbf{X}$ is a $K\times K$ size matrix of transmitted signal, $\mathbf{h}$ is a $K\times 1$ complex Gaussian vector of channel coefficients with zero mean and covariance matrix $\mathbf{C}_{hh}$, and $\mathbf{n}$ is a $K\times 1$ complex AWGN vector with zero mean and covariance matrix $\mathbf{C}_n$. The noise vector $\mathbf{n}$ is uncorrelated with $\mathbf{h}$. The channel covariance matrix $\mathbf{C}_{hh}$ can be represented as

$$\mathbf{C}_{hh} = \begin{bmatrix} R_h(0) & R_h(T_s) & \cdots & R_h((K-1)T_s) \\ R_h(T_s) & R_h(0) & \cdots & R_h((K-2)T_s) \\ \vdots & \vdots & \ddots & \vdots \\ R_h((K-1)T_s) & R_h((K-2)T_s) & \cdots & R_h(0) \end{bmatrix} \tag{2.61}$$

where $R_h(kT_s) = J_0(2\pi f_d k T_s)$. The noise covariance matrix $\mathbf{C}_n = \sigma_n^2\mathbf{I}$, where $\mathbf{I}$ is a $K \times K$ identity matrix. According to [51], the LMMSE estimator of channel coefficients $\mathbf{h}$ can be expressed as

$$\hat{\mathbf{h}}_{LMMSE} = \mathbf{C}_{hh}\mathbf{X}^T(\mathbf{X}\mathbf{C}_{hh}\mathbf{X}^T + \mathbf{C}_n)^{-1}\mathbf{r}. \tag{2.62}$$

Although the LMMSE channel estimator can achieve optimal performance with known Doppler spread, it requires the matrix inverse operation which causes a high demand of computational complexity and can be a concern for practical applications.

2.8 Conclusion

In this Chapter, we presented a literature review of the fading channel properties and some existing Doppler spread estimation approaches. The significance of estimating Doppler spread as well as the mutual dependence of the fading channel and Doppler spread are also discussed in this Chapter. The issues of high complexity cost and performance degradation in low or high Doppler spread range in the existing approaches need to be solved. In this thesis, we aim to devise a low-complexity joint Doppler spread and channel estimation approach with good performance over a wide range of the maximum Doppler frequency.

Chapter 3

Iterative Doppler Spread and Channel Estimation

3.1 Introduction

The knowledge of Doppler spread can be used to characterise the time variation of the fading channels [3, 13, 33, 49], and it can be employed to improve the channel estimation performance. In the literature, some channel estimation approaches simply assume that the Doppler spread is known at the receiver [45–48]. On the other hand, some Doppler spread estimation approaches assume that the channel estimates are available [3, 5, 13, 24, 29, 30, 32, 33, 36, 42, 44]. The mutual dependence of Doppler spread estimation and channel estimation motivated joint Doppler spread and channel estimation to achieve better performance. To this end, an expectation-maximization (EM) based approach [10] was proposed by using a Taylor series expansion based channel model. However, the complexity of this approach can be a concern. Alternatively, based on an autoregressive (AR) model for the time-varying fading channel, an EM based joint channel and AR model coefficient estimation approach was proposed in [11], where the Doppler

spread can be extracted from the estimated AR model coefficient.

In this Chapter, we propose a new joint Doppler spread and channel estimation approach for Rayleigh fading channels through an iterative process between a Doppler spread estimator and a channel estimator. We devise an autocorrelation function (ACF) lag selection mechanism for our ACF based Doppler spread estimator, and the ACF lag selection mechanism is crucial to maximise the performance of Doppler spread estimation. The low-complexity channel estimator is implemented using Gaussian message passing (GMP) techniques with a Forney-style factor graph (FFG) representation of time-varying channel characterised by a first order autoregressive (AR(1)) model. In addition, the Doppler spread estimate is used to optimise the AR(1) channel model coefficients to further enhance the performance of channel estimation. Compared to the EM approach in [10], the proposed approach delivers similar or better performance with significantly lower complexity. Compared to the EM approach in [11], the proposed approach has similar complexity per iteration, but the convergence of the proposed approach is much faster than that in [11], and the performance of the proposed approach is better than that of [11].

The rest of this Chapter is organised as follows. We first give an brief introduction to factor graphs and GMP techniques. Next, we use an FFG to represent the fading channel which is described by an AR(1) model, and implement the GMP techniques for the proposed iterative Doppler spread and channel estimation approach. After that, we compare the proposed approach with other approaches in terms of computational complexity. Finally, we give a conclusion of this Chapter.

3.2 Introduction of Factor Graph and Gaussian Message Passing

In this section, we first briefly introduce the factor graphs and the sum-product algorithm running on the factor graphs to find the marginalisation of a variable in a global function. Then, we focus on a special case of graphs where all the involved variables are Gaussian distributed. After that, we introduce the GMP technique and its updating rules in the basic FFGs.

3.2.1 An Introduction to Factor Graph and the Sum-Product Algorithm

In recent years, factor graphs are growing more useful for the design of algorithms to model-based detection and estimation problems involving many variables [52]. The applications of factor graphs to represent complicated global functions of many variables and the marginalization of these functions by means of the sum-product algorithm have attracted much attention.

In this thesis, we use FFGs where edges represent variables and boxes represent factors. In general, an FFG is composed of nodes (denoted by boxes), edges and half edges (connected only to one node). The factors are sometimes called local functions (e.g., $\{f_i\}$ in (3.1)) and their product is called global function (e.g., f in (3.1)). For example, a function $f(x_1, x_2, x_3, x_4, x_5)$ can be factored as

$$f(x_1, x_2, x_3, x_4, x_5) = f_1(x_1) f_2(x_1, x_2, x_3) f_3(x_3) f_4(x_2, x_4, x_5), \tag{3.1}$$

which is represented by the FFG shown in Fig. 3.1.

The FFG is defined by the following rules [52]:

- There is a unique node for each factor;

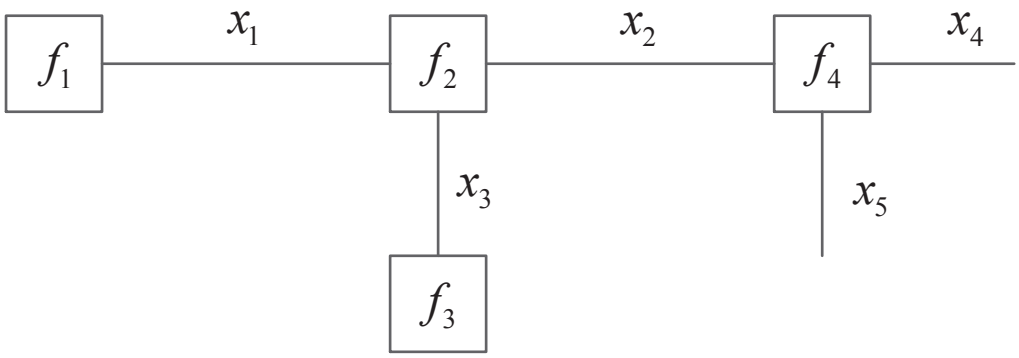

Figure 3.1: Forney-style factor graph representation of (3.1).

- There is a unique edge or half edge for each variable;
- Each node representing a factor g is connected with the edge (or/and half edge) representing some variables $\{x_i\}$ if and only if g is a function of $\{x_i\}$.

The above rules mean that no variable appears in more than two factors. In fact, it can be guaranteed by introducing the equality constraint function shown below

$$f_=(x_1, x_2, x_3) = \delta(x_1 - x_2)\delta(x_1 - x_3), \tag{3.2}$$

where $\delta(\cdot)$ is the Dirac delta function in the case of continuous variables and Kronecker delta function in the case of discrete variables. The FFG of the equality node is shown in Fig. 3.2. Equality nodes can allow more than two factors to share the same variable.

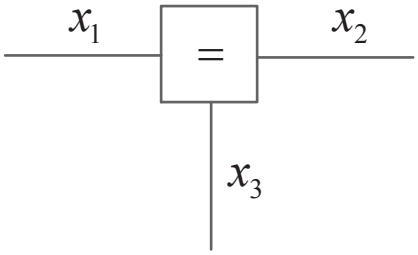

Figure 3.2: An equality constraint node.

A main application of factor graphs is for stochastic models. The following is an example. Let x be a random variable. y_1 and y_2 are two independent observations of x interrupted by noise. The joint probability distribution of these variables is [52]

$$p(x, y_1, y_2) = p(x)p(y_1|x)p(y_2|x), \tag{3.3}$$

which is represented by the FFG shown in Fig. 3.3. Actually, Fig. 3.3 shows an extended model with auxiliary variables x' and x'' where the joint probability density can be expressed as

$$p(x, x', x'', y_1, y_2) = p(x)p(y_1|x)p(y_2|x)f_=(x, x', x''). \tag{3.4}$$

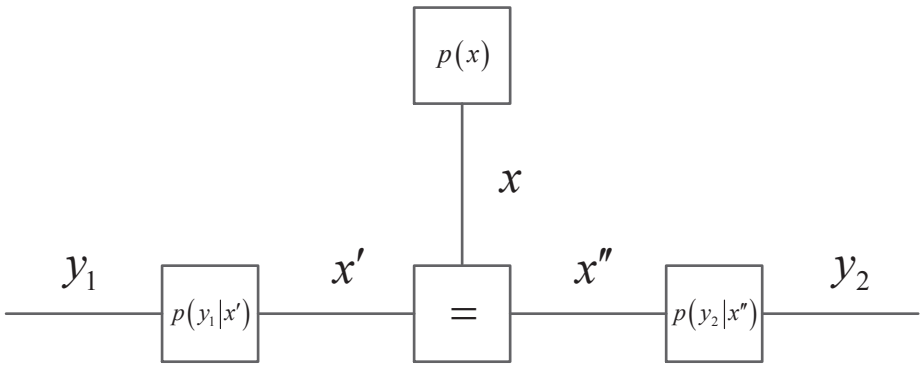

Figure 3.3: The FFG representation of (3.3) and (3.4).

The FFG has the following advantages [53]:

- It is suited for hierarchical modeling;
- It is compatible with standard block diagrams;
- It has the simplest formulation of the summary-product message update rule.

In the following sections, we discuss how the sum-product algorithm runs in the factor graph to obtain the marginalisation of a variable in the global function. For some given global function $f(x_1, \cdots, x_K)$, assume that we wish to compute the marginalisation of one variable x_k

$$\bar{f}_k(x_k) = \sum_{\substack{x_1,\cdots,x_K \\ except\ x_k}} f(x_1, \cdots, x_K). \tag{3.5}$$

If $f(x_1, \cdots, x_K)$ has a cycle-free factor graph, the marginalization (**??**) can be exactely computed by using the sum-product algorithm that splits a "big" marginalization into a sequence of "small" marginalisations [52]. We consider the following example. Assume that the global function $f(x_1, \cdots, x_7)$ can be factored as

$$f(x_1, \cdots, x_7) = f_1(x_1)f_2(x_1, x_2, x_3)f_3(x_3)f_4(x_2, x_4, x_5)f_5(x_5)f_6(x_4, x_6, x_7)f_7(x_7), \tag{3.6}$$

and its factor graph is shown in Fig. 3.4, where arrows are used to indicate the directions of the messages. Suppose that we wish to compute the marginalization of x_2,

$$\bar{f}_2(x_2) = \sum_{\substack{x_1,\cdots,x_7 \\ except\ x_2}} f(x_1, \cdots, x_7). \tag{3.7}$$

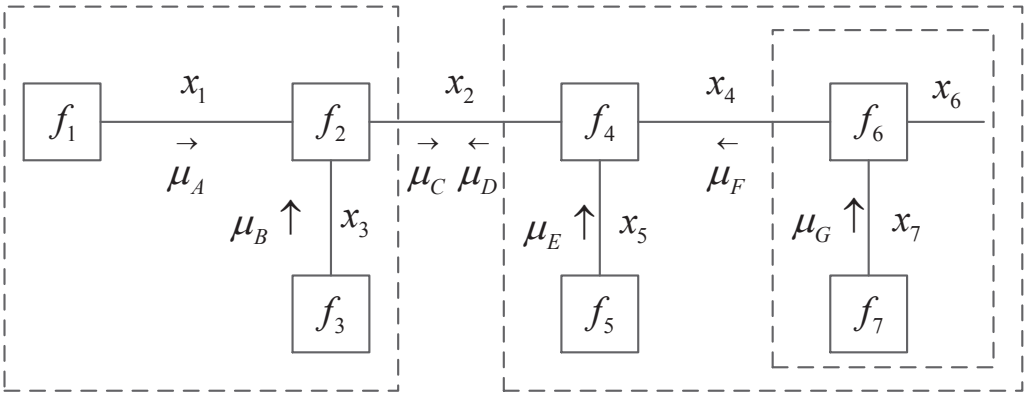

Figure 3.4: Illustration of message passing in the factor graph of (3.6).

We can easily verify that

$$\bar{f}_2(x_2) = \mu_C(x_2)\mu_D(x_2), \tag{3.8}$$

where

$$\mu_C(x_2) = \sum_{x_1,x_3} f_2(x_1, x_2, x_3)\mu_A(x_1)\mu_B(x_3), \tag{3.9}$$

$$\mu_D(x_2) = \sum_{x_4,x_5} f_4(x_2, x_4, x_5)\mu_E(x_5)\mu_F(x_4), \tag{3.10}$$

with

$$\mu_A(x_1) = f_1(x_1), \tag{3.11}$$

$$\mu_B(x_3) = f_3(x_3), \tag{3.12}$$

$$\mu_E(x_5) = f_5(x_5), \tag{3.13}$$

$$\mu_F(x_4) = \sum_{x_6,x_7} f_6(x_4, x_6, x_7)\mu_G(x_7), \tag{3.14}$$

and

$$\mu_G(x_7) = f_7(x_7). \tag{3.15}$$

We can see that μ_C and μ_D are the summaries of the dashed box in Fig. **??**, and μ_F is the marginalisation of x_4 in the local function f_6 and f_7. It can be found that all

the messages and summaries in (3.9)-(3.15) are formed according to the following sum-product rule.

Sum-Product Rule: The message out of some node (factor) f_l along some edge x_k is formed as the product of f_l and all incoming messages along all edges except x_k, summed over all involved variables except x_k [52]. From this example, it can be seen that the marginal $\bar{f}_k(x_k)$ may be obtained simultaneously by combining the two messages in both directions for every edge in the factor graph.

Since the sum-product rule is a "local" computation, it can also be applied to factor graphs with cycles. The sum-product algorithm becomes an iterative algorithm where messages are recomputed according to some schedule until some stopping criterion is satisfied [52].

3.2.2 Gaussian Message Passing

The GMP technique provides a factor graph based signal processing approach for linear systems. An FFG of a linear system can be constructed using the basic building blocks: equality constraints, adders and multipliers. The sum-product message computation rules for such nodes preserve Gaussianity: if the incoming messages are members of the exponential family, then so are the outgoing messages. Hence, the messages passed in a linear model are all Gaussian. Since Gaussian distributions can be described either by mean vector $\mathbf{m}$ and the covariance matrix $\mathbf{V}$ (or by the weight matrix $\mathbf{W} \triangleq \mathbf{V}^{-1}$ and the transformed mean $\mathbf{Wm}$), the message computation in factor graphs can be expressed in the form of updating of these quantities. The GMP updating rules were first proposed in [54]. However, the direct application of these rules may incur high complexity due to

the involved matrix inversions. The enhanced GMP updating rules were developed and presented in [52] based on which we can develop more computationally efficient algorithms. In this thesis, we only select some related building blocks and their computation rules. Through local computations based on the GMP updating rules, the global information (means and variances) of the variables can be obtained. For notation convenience, we use the same convention in [52]. Let x be a variable, represented by a directed edge, i.e., an edge with an arrow, in an FFG. We use $\overrightarrow{\mathbf{m}}_x$ and $\overrightarrow{\mathbf{V}}_x$ to denote the mean vector and covariance matrix of the message that flows in the direction of the edge, while $\overleftarrow{\mathbf{m}}_x$ and $\overleftarrow{\mathbf{V}}_x$ are for the message in the opposite direction. If the factor graph has no cycles, the marginal global function is the Gaussian with mean $\mathbf{m}_x$ and covariance matrix $\mathbf{V}_x = \mathbf{W}_x^{-1}$ given by [52]

$$\mathbf{W}_x = \overrightarrow{\mathbf{W}}_x + \overleftarrow{\mathbf{W}}_x \tag{3.16}$$

and

$$\mathbf{W}_x\mathbf{m}_x = \overrightarrow{\mathbf{W}}_x\overrightarrow{\mathbf{m}}_x + \overleftarrow{\mathbf{W}}_x\overleftarrow{\mathbf{m}}_x. \tag{3.17}$$

Sometimes we will use the auxiliary quantity

$$\tilde{\mathbf{W}}_x = (\overrightarrow{\mathbf{V}}_x + \overleftarrow{\mathbf{V}}_x)^{-1} \tag{3.18}$$

which is dual to $\mathbf{V}_x = (\overrightarrow{\mathbf{W}}_x + \overleftarrow{\mathbf{W}}_x)^{-1}$. Some relations among these quantities are given as

$$\tilde{\mathbf{W}}_x = \overrightarrow{\mathbf{W}}_x\mathbf{V}_x\overleftarrow{\mathbf{W}}_x = \overrightarrow{\mathbf{W}}_x - \overrightarrow{\mathbf{W}}_x\mathbf{V}_x\overleftarrow{\mathbf{W}}_x, \tag{3.19}$$

$$\mathbf{V}_x = \overrightarrow{\mathbf{V}}_x\tilde{\mathbf{W}}_x\overleftarrow{\mathbf{V}}_x = \overrightarrow{\mathbf{V}}_x - \overrightarrow{\mathbf{V}}_x\tilde{\mathbf{W}}_x\overleftarrow{\mathbf{V}}_x, \tag{3.20}$$

$$\mathbf{m}_x = \mathbf{V}_x\overrightarrow{\mathbf{W}}_x\overrightarrow{\mathbf{m}}_x + \mathbf{V}_x\overleftarrow{\mathbf{W}}_x\overleftarrow{\mathbf{m}}_x = \overrightarrow{\mathbf{m}}_x - \overrightarrow{\mathbf{V}}_x\tilde{\mathbf{W}}_x\overrightarrow{\mathbf{m}}_x + \mathbf{V}_x\overleftarrow{\mathbf{W}}_x\overleftarrow{\mathbf{m}}_x. \tag{3.21}$$

The basic building blocks and their computation rules are listed in Table 3.1.

Table 3.1: GMP Computation Rules for Basic Building Blocks

Blocks	Rules	
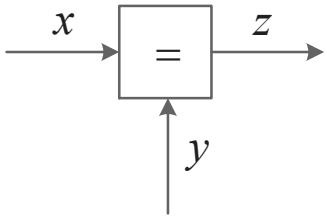	$\overrightarrow{\mathbf{W}}_z = \overrightarrow{\mathbf{W}}_x + \overrightarrow{\mathbf{W}}_y$	(3.22a)
	$\overleftarrow{\mathbf{W}}_x = \overleftarrow{\mathbf{W}}_z + \overrightarrow{\mathbf{W}}_y$	(3.22b)
	$\overrightarrow{\mathbf{W}}_z\overrightarrow{\mathbf{m}}_z = \overrightarrow{\mathbf{W}}_x\overrightarrow{\mathbf{m}}_x + \overrightarrow{\mathbf{W}}_y\overrightarrow{\mathbf{m}}_y$	(3.22c)
	$\overleftarrow{\mathbf{W}}_x\overleftarrow{\mathbf{m}}_x = \overleftarrow{\mathbf{W}}_z\overleftarrow{\mathbf{m}}_z + \overrightarrow{\mathbf{W}}_y\overrightarrow{\mathbf{m}}_y$	(3.22d)
	$\mathbf{m}_x = \mathbf{m}_y = \mathbf{m}_z$	(3.22e)
	$\mathbf{V}_x = \mathbf{V}_y = \mathbf{V}_z$	(3.22f)
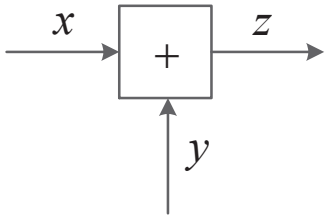	$\overrightarrow{\mathbf{V}}_z = \overrightarrow{\mathbf{V}}_x + \overrightarrow{\mathbf{V}}_y$	(3.23a)
	$\overleftarrow{\mathbf{V}}_x = \overleftarrow{\mathbf{V}}_z + \overrightarrow{\mathbf{V}}_y$	(3.23b)
	$\overrightarrow{\mathbf{m}}_z = \overrightarrow{\mathbf{m}}_x + \overrightarrow{\mathbf{m}}_y$	(3.23c)
	$\overleftarrow{\mathbf{m}}_x = \overleftarrow{\mathbf{m}}_z - \overrightarrow{\mathbf{m}}_y$	(3.23d)
	$\mathbf{m}_x + \mathbf{m}_y - \mathbf{m}_z = 0$	(3.23e)
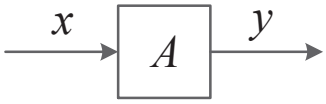	$\overrightarrow{\mathbf{V}}_y = \mathbf{A}\overrightarrow{\mathbf{V}}_x\mathbf{A}^H$	(3.24a)
	$\overrightarrow{\mathbf{m}}_y = \mathbf{A}\overrightarrow{\mathbf{m}}_x$	(3.24b)
	$\mathbf{V}_y = \mathbf{A}\mathbf{V}_x\mathbf{A}^H$	(3.24c)
	$\mathbf{m}_y = \mathbf{A}\mathbf{m}_x$	(3.24d)
	$\overleftarrow{\mathbf{W}}_x = \mathbf{A}^H\overleftarrow{\mathbf{W}}_y\mathbf{A}$	(3.24e)
	$\overleftarrow{\mathbf{W}}_x\overleftarrow{\mathbf{m}}_x = \mathbf{A}^H\overleftarrow{\mathbf{W}}_y\overleftarrow{\mathbf{m}}_y$	(3.24f)
	$\tilde{\mathbf{W}}_x = \mathbf{A}^H\tilde{\mathbf{W}}_y\mathbf{A}$	(3.24g)
	$\tilde{\mathbf{W}}_x\mathbf{m}_x = \mathbf{A}^H\tilde{\mathbf{W}}_y\mathbf{m}_y$	(3.24h)

3.3 Iterative Doppler Spread and Channel Estimation Approach

3.3.1 System Model

As in [3, 10, 13, 33, 49], we consider flat Rayleigh fading channels. Here, we mention that, if we adopt the tap-by-tap channel estimation strategy in [45], the proposed approach can be readily extended to the case of frequency selective

channels. The received baseband signal at time instant k can be represented as

$$r_k = h_k x_k + n_k, \qquad k = 0, 1, \cdots, K-1 \tag{3.25}$$

where the channel coefficient h_k is complex Gaussian distributed, x_k is the transmitted symbol and n_k is a zero-mean complex additive white Gaussian noise (AWGN) with variance σ_n^2. The Rayleigh fading channels are assumed to follow the Jakes model [12], and the normalised channel ACF can be expressed as

$$R_h(lT_s) = J_0(2\pi f_d l T_s) \tag{3.26}$$

where $l \in \{0, 1, 2 \cdots\}$, T_s is the sampling period, lT_s is the ACF lag, f_d is the maximum Doppler frequency and $J_0(\cdot)$ is the zeroth order Bessel function of the first kind.

The objective of this work is to jointly estimate f_d and $\{h_k\}$ using pilot symbols $\{x_k\}$. For the sake of simplicity, we assume $x_k = 1$ where $k = 0, 1, \cdots, K-1$. It should be noted that pilot symbols can be periodically inserted into data symbols. In this case, $\{x_k\}$ in model (3.25) is a mix of data and pilot symbols. In this work, we only consider estimating channel coefficients at pilot positions. Channel coefficients at data positions can be obtained based on the channel estimates at pilot positions, e.g., through interpolation, which is out of the scope of this work.

As shown in Fig. 3.5, the proposed approach includes a Doppler spread estimator and a channel estimator, which work iteratively. The output $\left\{\hat{h}_k\right\}$ of the channel estimator is used by the Doppler spread estimator to produce an estimate of the maximum Doppler frequency $\hat{f_d}$. Then $\hat{f_d}$ is used by the channel estimator to obtain refined channel estimates in the next iteration.

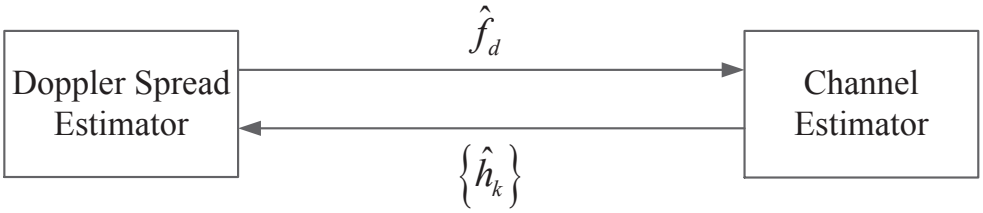

Figure 3.5: Block diagram of the proposed iterative Doppler spread and channel estimation approach.

3.3.2 ACF Based Doppler Spread Estimation

The Doppler spread estimation is based on the channel ACF, given in (3.26). However, $R_h(lT_s) = J_0(2\pi f_d l T_s)$ is not a monotonic function of f_d. Define $J_0^{-1}(\cdot)$ as the inverse function of $J_0(\cdot)$ in its first monotonous range. Then the maximum Doppler frequency can be expressed as

$$\hat{f_d} = \frac{J_0^{-1}(R_h(lT_s))}{2\pi l T_s}. \tag{3.27}$$

The estimate of $R_h(lT_s)$ can be obtained based on the channel estimates $\{\hat{h}_k\}$ which are available from the channel estimator. Then f_d can be estimated using (3.27). The implementation of the above Doppler spread estimation requires the knowledge of l. It is noted that we need to select a proper value of l to maximise the Doppler spread estimation performance.

3.3.2.1 ACF Lag Selection Mechanism

The zeroth order Bessel function of the first kind $J_0(x)$ is shown in Fig. 3.6. As $J_0(x)$ is a non-linear function, it affects the accuracy of Doppler spread estimation in two aspects. One aspect is that the zeroth order Bessel function is not a one to one map function. Given the value of $J_0(x)$, it may have several corresponding variables x. Therefore, we need to make sure that $x = 2\pi f_d l T_s$ is in the first

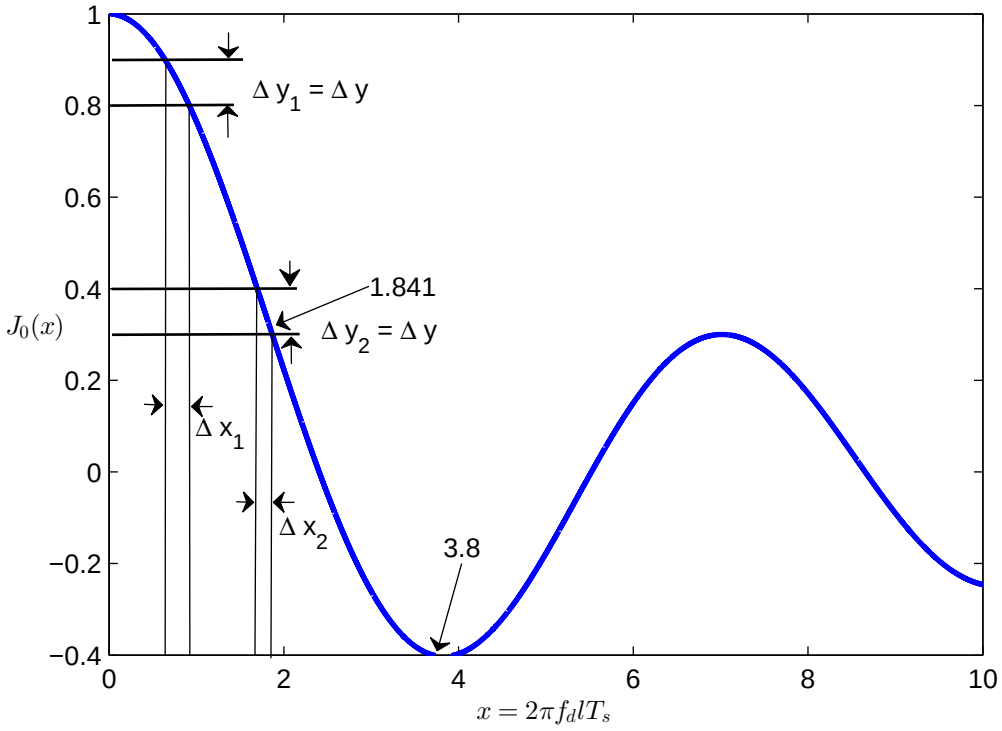

Figure 3.6: The zeroth order Bessel function of the first kind

monotonous range of $J_0(x)$, i.e., $0 \leq x \leq 3.8$. The other aspect is that the slope of $J_0(x)$ varies with $x = 2\pi f_d l T_s$. It is obvious in Fig. 3.6 that with the same estimation offset $\Delta y_1 = \Delta y_2 = \Delta y$, the variances of the estimated maximum Doppler frequency are different at various x. To be specific, the slope of Δy_1 is smaller than that of Δy_2, while the estimation variance Δx_1 is larger than Δx_2, which leads to a conclusion that in the first monotonous range of $J_0(x)$, a small gradient of $J_0(2\pi f_d l T_s)$ causes a large estimation error of the maximum Doppler frequency. In order to maximise the Doppler spread estimation performance, we choose a value l_* so that $x = 2\pi f_d l_* T_s$ is closest to the point with the greatest slope of $J_0(x)$. As $x \approx 1.841$, $J_0(x)$ has the largest slope. Therefore, l can be expressed as

$$l = round\left[\frac{1.841}{2\pi f_d T_s}\right]. \tag{3.28}$$

The implementation of the above selection method requires the knowledge of

f_d. We can overcome this problem by taking advantage of the iterative process, i.e., we can use the estimate of f_d in the last iteration for selection l in the current iteration. For the first iteration, we can roughly select a value of l. Because the range of the maximum Doppler frequency is normally available, i.e., $f_d \in [0, F]$, we can simply use F to select the value of l using (3.28).

We note that $J_0(\cdot)$ in (3.27) can be implemented by a lookup table for $J_0(x)$. As x belongs to the first monotonous range of $J_0(x)$, $x = 2\pi f_d l T_s \in [0, 3.8]$. However, due to our proposed ACF lag selection mechanism, $x = 2\pi f_d l T_s$ will likely appear in the small range around 1.841. To reduce the table size, we use variable granularity. For example, we can divide the first monotonous range into three intervals, i.e., $0 \leq x \leq 1.6$, $1.61 \leq x \leq 1.99$ and $2.0 \leq x \leq 3.8$ with granularity 0.1, 0.01 and 0.1 respectively. In total, the lookup table has only 75 entries.

3.3.3 GMP Based Channel Estimation

The Rayleigh fading channel due to Clarke model [17] and its simplified simulation model due to Jakes [12] are the most accepted statistic model to describe the fading process of the complex baseband channel in wireless communications. However, this model is not convenient for channel estimation or equalisation. Conventionally, AR model is used to approximate the fading channel and facilitate its manipulation [55]. As in [55–57], we use an AR(1) model to approximately characterise the time-varying Rayleigh fading channel

$$h_k = \alpha h_{k-1} + g w_k, \quad k = 1, 2, \cdots, K-1 \tag{3.29}$$

where α and g are constants, and w_k is a zero mean complex white Gaussian noise with unit variance. Although an higher order of the AR model can achieve a

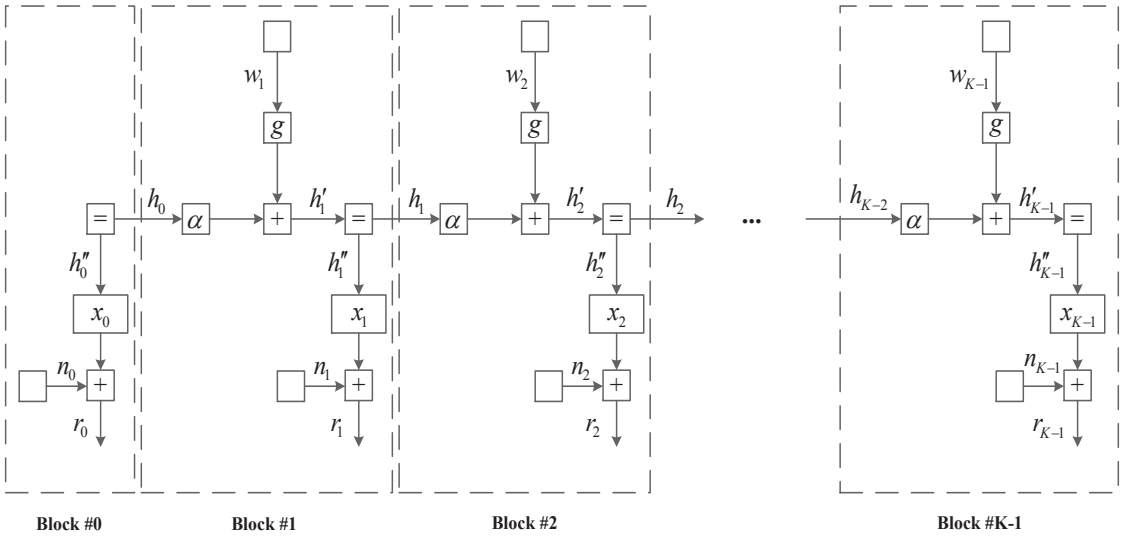

Figure 3.7: Factor graph of the Rayleigh fading channel with AR(1) model.

better approximation of the actual fading statistics, it also leads to higher computational complexity. In [49, 55, 57, 58], it draws a conclusion that AR(1) model approximation is enough to capture most of the dynamics of the actual fading process.

We employ the GMP technique [52] for channel estimation. The FFG representation of (3.25) and (3.29) is shown in Fig. 3.7. The FFG composes of K blocks, where Block #0 only includes the observation. Note that all variables in the FFG are scalars and the FFG has a tree structure, so the GMP provides the exact minimum mean square error (MMSE) estimate of each h_k based on all observations and the AR(1) model in (3.29) through local computations.

Following the convention in [52], we use a direct edge to denote a variable and use arrows to denote the directions of message passing. For example, in Fig. 3.7, we use $\overrightarrow{m}_{h_k}$ and $\overrightarrow{V}_{h_k}$ to denote the mean and variance of the message that flows in the direction of the edge, while $\overleftarrow{m}_{h_k}$ and $\overleftarrow{V}_{h_k}$ are for the message in the opposite

direction. The marginal message is denoted by m_{h_k} and V_{h_k}. $\{m_{h_k}, V_{h_k}\}$ are obtained by combining $\left\{\overrightarrow{m}_{h_k}, \overrightarrow{V}_{h_k}\right\}$ and $\left\{\overleftarrow{m}_{h_k}, \overleftarrow{V}_{h_k}\right\}$, which are produced through a forward recursion and a backward recursion respectively.

- **Forward Recursion**: Assume that $\left\{\overrightarrow{m}_{h_{k-1}}, \overrightarrow{V}_{h_{k-1}}\right\}$ are available from the blocks left to Block #k. In this process, we compute the message $\left\{\overrightarrow{m}_{h_k}, \overrightarrow{V}_{h_k}\right\}$ based on $\left\{\overrightarrow{m}_{h_{k-1}}, \overrightarrow{V}_{h_{k-1}}\right\}$ and $\left\{\overleftarrow{m}_{h''_k}, \overleftarrow{V}_{h''_k}\right\}$. Using (3.23) and (3.24) in Table 3.1, $\left\{\overrightarrow{m}_{h'_k}, \overrightarrow{V}_{h'_k}\right\}$ can be expressed as

$$\overrightarrow{m}_{h'_k} = \alpha \overrightarrow{m}_{h_{k-1}} \tag{3.30a}$$

$$\overrightarrow{V}_{h'_k} = \alpha^2 \overrightarrow{V}_{h_{k-1}} + g^2. \tag{3.30b}$$

  Applying (3.22) in Table 3.1, the message $\left\{\overrightarrow{V}_{h_k}, \overrightarrow{m}_{h_k}\right\}$ can be calculated as

$$\overrightarrow{V}_{h_k} = \left(\overrightarrow{V}^{-1}_{h'_k} + \overleftarrow{V}^{-1}_{h''_k}\right)^{-1} \tag{3.31a}$$

$$\overrightarrow{m}_{h_k} = \overrightarrow{V}_{h_k}\left(\frac{\overrightarrow{m}_{h'_k}}{\overrightarrow{V}_{h'_k}} + \frac{\overleftarrow{m}_{h''_k}}{\overleftarrow{V}_{h''_k}}\right) \tag{3.31b}$$

  where $\left\{\overleftarrow{m}_{h''_k}, \overleftarrow{V}_{h''_k}\right\}$ can be obtained using (3.23) and (3.24),

$$\overleftarrow{m}_{h''_k} = \frac{\overleftarrow{m}_{r_k}}{x_k} = r_k \tag{3.32a}$$

$$\overleftarrow{V}_{h''_k} = \frac{\overrightarrow{V}_{n_k}}{x_k^2} = \sigma_n^2. \tag{3.32b}$$

  According to the GMP updating rules in (3.22), we have $\overrightarrow{m}_{h_0} = r_0$ and $\overrightarrow{V}_{h_0} = \sigma_n^2$ for Block #0.

- **Backward Recursion**: Assume that $\left\{\overleftarrow{m}_{h_k}, \overleftarrow{V}_{h_k}\right\}$ which are available from the blocks right to Block #k. In this process, we compute the message $\left\{\overleftarrow{m}_{h_{k-1}}, \overleftarrow{V}_{h_{k-1}}\right\}$ based on $\left\{\overleftarrow{m}_{h_k}, \overleftarrow{V}_{h_k}\right\}$ and $\left\{\overleftarrow{m}_{h''_k}, \overleftarrow{V}_{h''_k}\right\}$. Using (3.22), $\left\{\overleftarrow{V}_{h'_k}, \overleftarrow{m}_{h'_k}\right\}$ can

be calculated as

$$\overleftarrow{V}_{h'_k} = \left(\overleftarrow{V}_{h_k}^{-1} + \overleftarrow{V}_{h''_k}^{-1}\right)^{-1} \tag{3.33a}$$

$$\overleftarrow{m}_{h'_k} = \overleftarrow{V}_{h'_k}\left(\frac{\overleftarrow{m}_{h_k}}{\overleftarrow{V}_{h_k}} + \frac{\overleftarrow{m}_{h''_k}}{\overleftarrow{V}_{h''_k}}\right) \tag{3.33b}$$

where $\left\{\overleftarrow{m}_{h''_k}, \overleftarrow{V}_{h''_k}\right\}$ are given by (3.32). Applying (3.23) and (3.24), $\left\{\overleftarrow{V}_{h_{k-1}}, \overleftarrow{m}_{h_{k-1}}\right\}$ can be represented as

$$\overleftarrow{V}_{h_{k-1}} = \frac{\overleftarrow{V}_{h'_k} + g^2}{\alpha^2} \tag{3.34a}$$

$$\overleftarrow{m}_{h_{k-1}} = \frac{\overleftarrow{m}_{h'_k}}{\alpha}. \tag{3.34b}$$

According to the GMP updating rules in (3.22), we have $\overleftarrow{m}_{h'_{K-1}} = r_{K-1}$ and $\overleftarrow{V}_{h'_{K-1}} = \sigma_n^2$ for Block $\#K-1$. Here, we note that the messages $\left\{\overleftarrow{m}_{h''_k}, \overleftarrow{V}_{h''_k}\right\}$ are based on the observations and do not change during the iteration, i.e., (3.32) only need to be calculated once.

- **Output Messages**: After the forward and backward recursions, $\left\{\overrightarrow{m}_{h_k}, \overrightarrow{V}_{h_k}\right\}$ and $\left\{\overleftarrow{m}_{h_k}, \overleftarrow{V}_{h_k}\right\}$ are available. By combining the forward and backward messages, the marginal mean scalar m_{h_k} can be represented as

$$m_{h_k} = \frac{\overrightarrow{m}_{h_k}\overrightarrow{V}_{h_k}^{-1} + \overleftarrow{m}_{h_k}\overleftarrow{V}_{h_k}^{-1}}{\overrightarrow{V}_{h_k}^{-1} + \overleftarrow{V}_{h_k}^{-1}} \tag{3.35}$$

which is used as the estimate of h_k.

It is noted that the above GMP algorithm assumes that α and g are known. They can be obtained based on the output of the Doppler spread estimator.

3.3.3.1 The Optimisation of AR(1) Model Coefficient

Conventionally, the values of α and g are determined by matching the ACFs of the $AR(1)$ model and the Jakes model at time lag T_s, yielding [56]

$$\alpha = \frac{R_h(T_s)}{R_h(0)} = J_0(2\pi f_d T_s) \tag{3.36}$$

$$g = \sqrt{1-\alpha^2}. \tag{3.37}$$

It has been revealed in [55, 57] that α in (3.36) is not optimal for channel estimation in terms of mean square error (MSE). The work in [55] gave an approximated closed-form expression for the optimal AR(1) model coefficient to minimise the MSE of channel estimation

$$\alpha_* = \sqrt{1 - 4\sqrt[3]{(\pi f_d T_s)^4 \frac{\sigma_n^2}{\sigma_h^2}}} \tag{3.38}$$

where σ_h^2 is the channel power. By substituting (3.38) into (3.37) we have g_*. In this thesis, we use (3.38) to calculate the AR(1) model coefficients based on $\hat{f}_d$ from the Doppler spread estimator.

As the AR(1) model coefficients are unknown in the first iteration, we can form the initialised channel estimates based on the received samples using (3.32), which are used as the input to the Doppler spread estimator. We summarise the proposed iterative Doppler spread and channel estimation approach in Table 3.2.

Table 3.2: Steps for the Proposed Iterative Doppler Spread and Channel Estimation Approach

- **Initialisation for the first iteration**:
  1. Form the initialised channel estimates using (3.32).
  2. Select the ACF lag based on the maximum Doppler frequency F using (3.28).
- **ACF Based Doppler spread estimation**:
  1. Estimate f_d by (3.27).
  2. Update the ACF lag by (3.28) for the next iteration.
  3. Calculate the optimised α_* by (3.38) for GMP based channel estimation.
- **GMP Based channel estimation**:
  1. Forward recursion: calculate $\left\{\overrightarrow{m}_{h_k}, \overrightarrow{V}_{h_k}\right\}$ for each block.
  2. Backward recursion: calculate $\left\{\overleftarrow{m}_{h_k}, \overleftarrow{V}_{h_k}\right\}$ for each block.
  3. Output message: calculate m_{h_k} which is used as the channel estimates and the input to the Doppler spread estimator by (3.35).
  4. Repeat iterative process between Doppler spread estimator and channel estimator until convergence.

3.4 Computational Complexity Comparison

The computational costs of the proposed approach and other approaches are provided in Table 3.3. Only multiplication operations are considered. The LMMSE channel estimator which requires the knowledge of Doppler spread to form the channel covariance matrix, has the complexity of $O(K^3)$. The sample covariance (SC) [13], suboptimal ML (SML) [3] and ML [3] approaches only provide Doppler spread estimates with complexities of $O((L+1)K)$, $O(K^2)$ and $O(K^3)$, respectively, where K is the number of pilots and L is the number of sample correlations used in [13]. The proposed approach and two EM approaches in [10] and [11], produce both Doppler spread and channel estimates. The complexity of the proposed

Table 3.3: Computational Complexity Comparison (K: the number of pilots; P=20; L=10)

Purpose	Approach	Complexity
Channel estimation only	LMMSE	$\mathcal{O}(K^3)$
Doppler spread estimation only	SC [13]	$\mathcal{O}((L+1)K)$
	SML [3]	$\mathcal{O}(K^2)$
	ML [3]	$\mathcal{O}(K^3)$
Joint channel and Doppler spread estimation	Proposed	$\mathcal{O}(20K)$ per iteration
	EM in [11]	$\mathcal{O}(17K)$ per iteration
	EM in [10]	$\mathcal{O}((P+1)^2K)$ per iteration

approach is significantly lower than the EM in [10], where the approximate order of the Taylor expansion based channel model $P = 10$ in [10] ($P = 20$ is used in the simulations of this work). The proposed approach has a similar complexity per iteration as the EM in [11]. However, the convergence of the proposed approach is much faster than that in [11] as shown in the simulation results.

3.5 Simulation Results

The system settings are as follows. The time-varying Rayleigh fading channel is generated using the method in [16]. We set the carrier frequency $f_c = 1.8$GHz, mobile speed $v \in [30\text{km/h}, 300\text{km/h}]$, so the maximum Doppler frequency $f_d \in [50\text{Hz}, 500\text{Hz}]$. The symbol duration is set as 10μs and the number of pilots symbols $K = 100$. Between two neighbouring pilot symbols, 9 data symbols are inserted for transmission. Thus the time interval between two neighbouring pilot symbols is $T_s = 100\mu$s. For comparison, the performance of LMMSE channel estimation approach, some existing Doppler spread estimation approaches such as ML [3], SML [3] and SC [13], and two EM based joint Doppler spread and channel estimation approaches in [10] and [11] are provided. We set $L = 10$ as

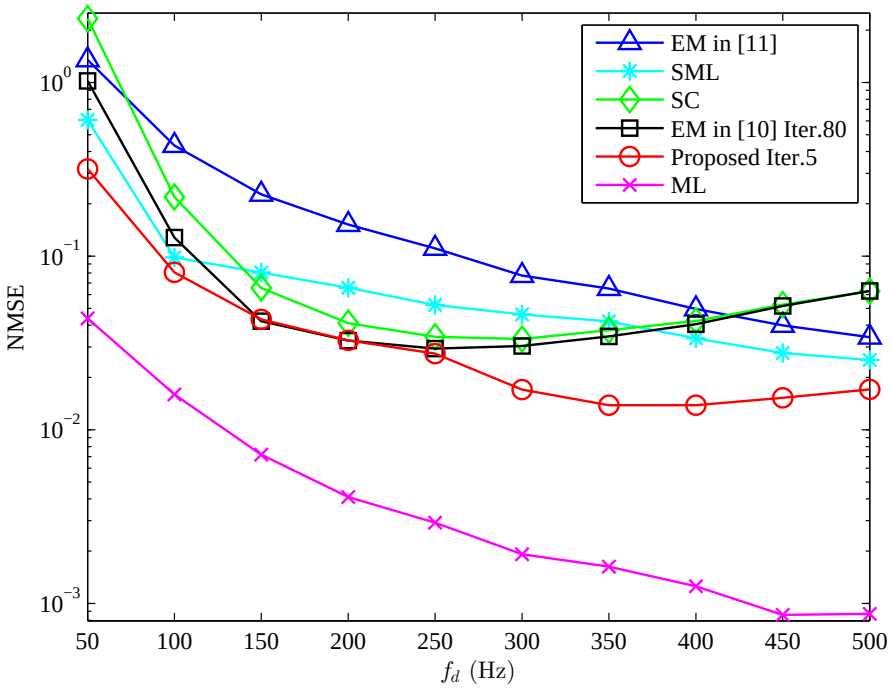

Figure 3.8: NMSE performance of Doppler spread estimation for $K = 100$ and SNR= 10dB.

the number of sample correlations for the SC approach in [13] and $P = 20$ as the approximate order of the Taylor expansion based channel model for the EM approach in [10].

The normalised MSE (NMSE) performance of Doppler spread estimation is shown in Fig. 3.8. The ML estimator achieves the best performance at the cost of the highest computational complexity. Here, we mention that the EM approach in [10] uses the estimated maximum Doppler frequency provided by the SC approach as the initialised value for the EM algorithm. The performance of the SC method and the EM in [10] degrades in high Doppler frequency range. The proposed approach achieves better performance over the SC, SML methods and the two EM approaches especially in the whole Doppler frequency range.

Fig. 3.9 shows the NMSE performance for Doppler spread estimation with

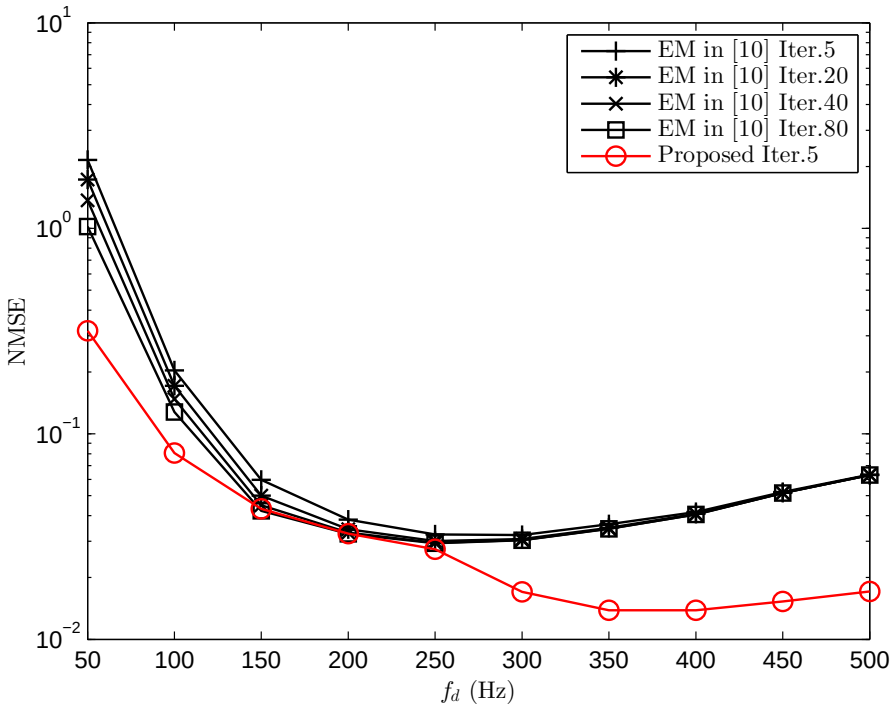

Figure 3.9: NMSE performance of Doppler spread estimation versus number of iterations with f_d = 100Hz, K = 100 and SNR= 10dB.

different number of iterations. It can be seen that the proposed approach with 5 iterations outperforms the EM approach in [10] with 5 or even 80 iterations. The reason of why the performance of the EM approach in [10] becomes worse at higher Doppler frequency is that there is no performance improvement in higher Doppler frequency with even more EM iterations. Note that the complexity of the proposed approach per iteration is much lower than that of the EM approach in [10]. Therefore, the proposed approach achieves better performance with considerably lower complexity than the EM approach in [10].

The MSE performance of channel estimation is shown in Fig. 3.10. The LMMSE channel estimator provides the optimal performance compared to other estimators, but it assumes that the knowledge of Doppler spread is available and the computational cost is much higher than other estimators. It is shown that

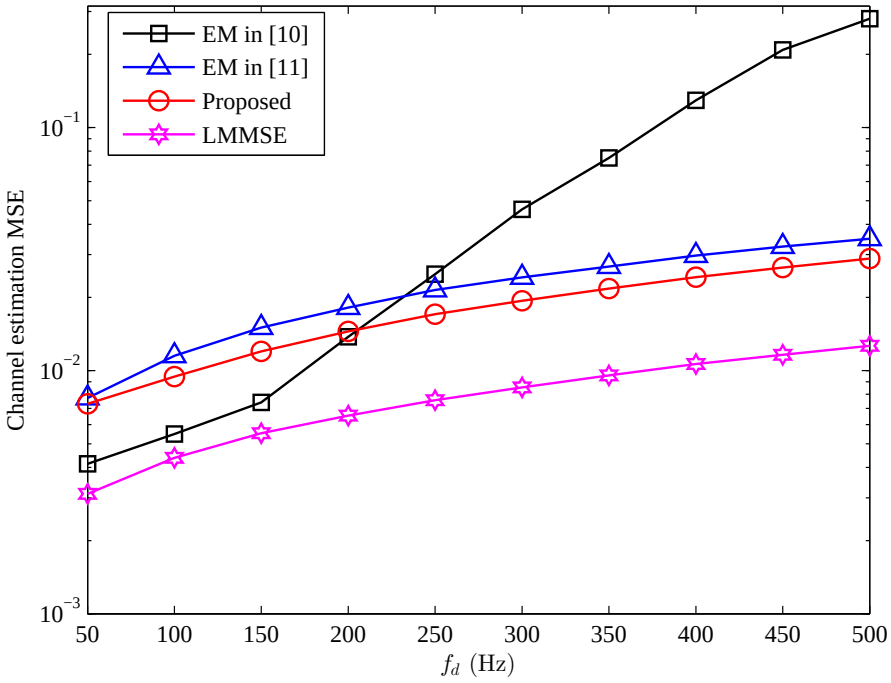

Figure 3.10: MSE performance of channel estimation for $K = 100$ and SNR= 10dB.

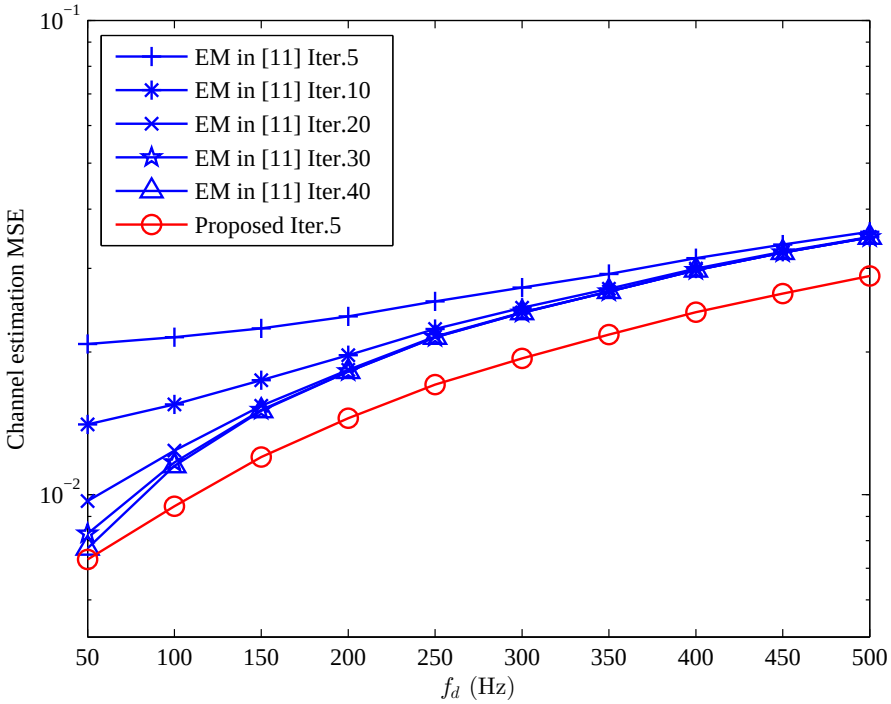

Figure 3.11: MSE performance of channel estimation with different iterations for $K = 100$ and SNR= 10dB.

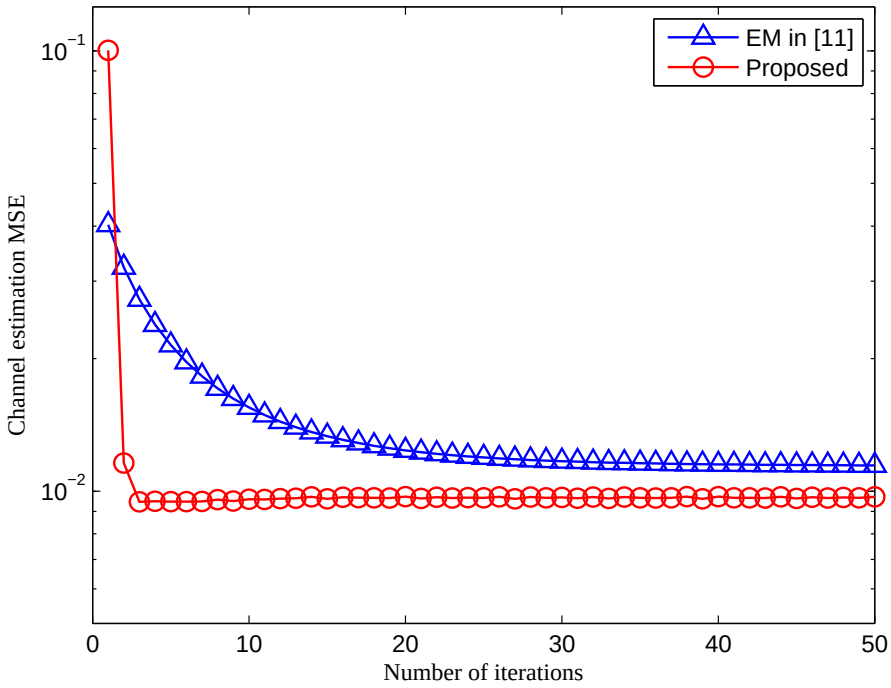

Figure 3.12: MSE versus number of iterations for channel estimation with f_d = 100Hz, K = 100 and SNR=10dB.

the EM approach in [10] gives highly biased channel estimates in high Doppler frequency range due to the biased Doppler spread estimates. It can be seen that in low Doppler frequency range, the EM in [10] has better performance than the proposed approach at the cost of much higher complexity. In medium to high Doppler frequency range, the proposed approach outperforms the EM in [10] with much lower complexity. The proposed approach achieves better performance than the EM in [11]. Fig. 3.11 shows the MSE performance for channel estimation of the proposed approach and the EM in [11] with different numbers of iterations. It can be seen that the proposed approach with 5 iterations achieves better performance compared with the EM in [11] even with 40 iterations. So the total complexity of the proposed approach is lower than that in [11]. In Fig. 3.12, we again demonstrate the fast convergence speed of the proposed approach.

3.6 Conclusion

In this Chapter, we proposed a new low-complexity iterative approach to joint Doppler spread and channel estimation over Rayleigh fading channels. Through an iterative process between two devised estimators, i.e., an ACF based Doppler spread estimator with an ACF lag selection mechanism and a GMP based channel estimator with a FFG representation of an optimised AR(1) channel model, we achieve similar or better performance with lower complexity compared to existing joint Doppler spread and channel estimation approaches.

Chapter 4

EM Based Time-Varying Channel Estimation

4.1 Introduction

It has been recently shown that the expectation-maximisation (EM) algorithm may be viewed as message passing in factor graphs [59], where the expectation step generates the EM messages to be used in the maximisation step. The EM messages may be obtained through a general local computation rule and the local expectations involved in the EM messages computation may be calculated by the sum-product message passing [59]. With the EM message from the expectation step, the maximisation step may be realised using the max-product message passing. In particular, for a linear Gaussian system with unknown parameters, the EM message turns out to be Gaussian and the implementation of EM algorithm can be achieved using the Gaussian message passing (GMP) technique.

In this Chapter, using a Forney-style factor graph (FFG) representation of the Rayleigh fading channels characterised by a first order autoregrssive (AR(1)) model with unknown coefficients, an EM based time-varying channel estimation

approach using GMP techniques is proposed, where the EM based proposed algorithm can provide the estimates of channel coefficients and AR(1) model coefficients. Doppler spread can be extracted from the estimated AR(1) model coefficients [11]. We first briefly introduce the EM algorithm as message passing. Then, we employ the EM message passing technique for time-varying channel estimation.

4.2 EM Algorithm Using Message Passing

In this section, we first review the EM algorithm. Then, we introduce the EM algorithm as message passing. After that, we discuss the EM message passing for linear Gaussian system and present the computation rules for the EM messages.

4.2.1 Review of EM Algorithm

The EM algorithm is an iterative technique for parameter estimation in a probabilistic model. Use vectors $\mathbf{r}$, $\mathbf{x}$ and $\boldsymbol{\theta}$ to denote observed data, hidden data and the unknown parameters to be estimated, respectively, and $f(\mathbf{r}, \mathbf{x}, \boldsymbol{\theta})$ to denote either a joint probability density function (PDF) of $\mathbf{r}$ and $\mathbf{x}$ parameterised by $\boldsymbol{\theta}$ or a joint PDF of $\mathbf{r}$, $\mathbf{x}$ and $\boldsymbol{\theta}$, the maximum likelihood estimate of the unknown parameters $\boldsymbol{\theta}$ can be represented as

$$\hat{\boldsymbol{\theta}} = \arg\max_{\boldsymbol{\theta}} \int_{\mathbf{x}} f(\mathbf{r}, \mathbf{x}, \boldsymbol{\theta}) \mathrm{d}\mathbf{x}. \tag{4.1}$$

The maximisation of $\boldsymbol{\theta}$ may be intractable and not feasible for practical implementation due to high complexity and exhaustive search. The EM algorithm involves two steps to solve this problem iteratively, and each iteration, e.g., the ith iteration, the two steps are expressed as follows:

- E-Step:

$$Q(\boldsymbol{\theta}|\hat{\boldsymbol{\theta}}^{(i-1)}) = \mathrm{E}\left[\log f(\mathbf{r}, \mathbf{x}, \boldsymbol{\theta})|\mathbf{r}, \hat{\boldsymbol{\theta}}^{(i-1)}\right]. \tag{4.2}$$

- M-Step:

$$\hat{\boldsymbol{\theta}}^{(i)} = \arg\max_{\boldsymbol{\theta}} Q(\boldsymbol{\theta}|\hat{\boldsymbol{\theta}}^{(i-1)}). \tag{4.3}$$

Since $\boldsymbol{\theta}$ is unknown in the first iteration, an initialised value for $\hat{\boldsymbol{\theta}}^{(0)}$ is needed. Then, the EM algorithm carries out the E-step and M-step iteratively.

4.2.2 Message Passing EM Algorithm

We consider a nontrivial factorization

$$f(\mathbf{r}, \mathbf{x}, \boldsymbol{\theta}) = f_A(\boldsymbol{\theta}) f_B(\mathbf{r}, \mathbf{x}, \boldsymbol{\theta}) \tag{4.4}$$

where $\mathbf{r} = (r_1, \cdots, r_n)$, $\mathbf{x} = (x_1, \cdots, x_n)$ and $\boldsymbol{\theta} = (\theta_1, \cdots, \theta_n)$. Assume that f_B has a nontrivial factor graph, then the EM message $e^{\eta(\theta)}$ splits into messages $e^{\eta_1(\theta_1)}, e^{\eta_2(\theta_2)}, \cdots$ that can be computed "locally" in the factor graph of f_B. The maximum likelihood estimate in (4.1) can be rewritten as

$$\hat{\boldsymbol{\theta}} = \arg\max_{\boldsymbol{\theta}} f_A(\boldsymbol{\theta}) \int_{\mathbf{x}} f_B(\mathbf{r}, \mathbf{x}, \boldsymbol{\theta}) \mathrm{d}\mathbf{x} \tag{4.5}$$

where f_A and f_B can be represented by their corresponding factor graphs shown in Fig. 4.1, where the upper part is the graph corresponding to f_A, and the lower part is the graph corresponding to f_B. $\mathrm{e}^{\eta_l(\theta_l)}$ is the EM message.

The message passing EM algorithm [59] is as follows:

- Make some initial guess $\hat{\boldsymbol{\theta}}^{(0)} = (\hat{\theta}_1^{(0)}, \cdots, \hat{\theta}_n^{(0)})$.

- E-Step: With $\hat{\boldsymbol{\theta}}^{(i-1)}$ plugged into f_B, employ the sum-product message passing in the factor graph of f_B to calculate the messages for the local nodes

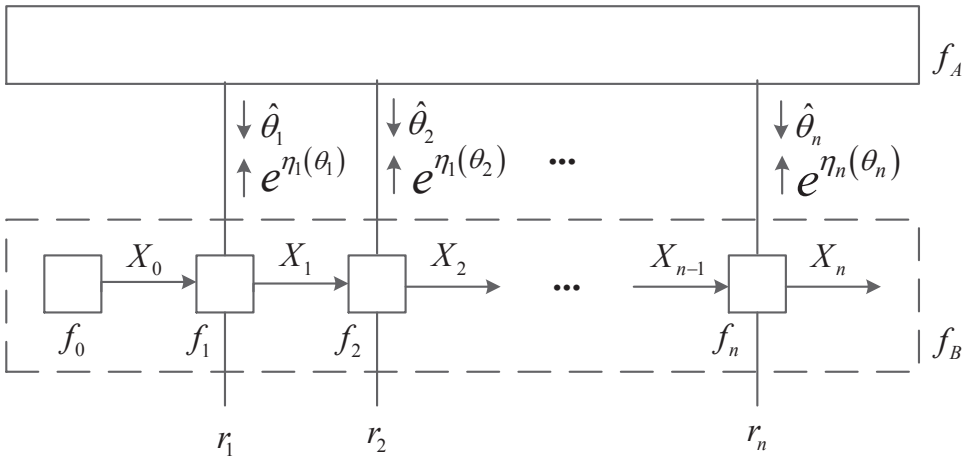

Figure 4.1: Application of EM to general state space model.

corresponding to θ_l. Then, compute the EM message $\mathrm{e}^{\eta_l(\hat{\theta}_l^{(i-1)})}$ which can be expressed as [59]

$$\begin{aligned}\eta_l(\hat{\theta}_l^{(i-1)}) &= \mathrm{E}_{\mathrm{p}_{local}}\left[f_l(X_{l-1}, X_l, r_l, \hat{\theta}_l^{(i-1)})\right] \\ &= \int_{x_{l-1},x_l} \mathrm{p}_{local}(x_{l-1}, x_l | r_l, \hat{\theta}_l^{(i-1)}) \cdot \log f_l(x_{l-1}, x_l, r_l, \hat{\theta}_l^{(i-1)}) \mathrm{d}x_{l-1}\mathrm{d}x_l\end{aligned} \tag{4.6}$$

with

$$\mathrm{p}_{local}(x_{l-1}, x_l | r_l, \hat{\theta}_l^{(i-1)}) \propto f_l(x_{l-1}, x_l, r_l, \hat{\theta}_l^{(i-1)}) \cdot \overrightarrow{\mu}_{X_{l-1}}(x_{l-1}) \overleftarrow{\mu}_{X_l}(x_l) \tag{4.7}$$

where $\overrightarrow{\mu}_{X_{l-1}}(x_{l-1})$ and $\overleftarrow{\mu}_{X_l}(x_l)$ denote the forward and backward sum-product message respectively.

- M-Step: With the EM messages from the E-step, employ the max-product message passing in the factor graph of f_A to obtain the new estimate $\hat{\boldsymbol{\theta}}^{(i)}$ which can be represented as

$$\hat{\boldsymbol{\theta}}^{(i)} = \underset{\theta_1,\cdots,\theta_n}{\arg\max}\, f_A(\theta_1, \cdots, \theta_n) \mathrm{e}^{\eta_1(\hat{\theta}_1^{(i-1)})} \cdots \mathrm{e}^{\eta_n(\hat{\theta}_n^{(i-1)})} \tag{4.8}$$

- Repeat the E-Step and M-Step until convergence.

4.2.3 EM for Linear Gaussian Systems

For a linear Gaussian system with unknown parameters, the sum-product messages of the E-step factor graph are Gaussian and can be computed by the GMP technique [52] (as introduced in Chapter 3). The unknown parameters and the missing data in such linear systems give rise to multiplier nodes in the factor graph of the system. It has been revealed in [59] that, with Gaussian incoming messages, the EM messages out of such multiplier nodes properly grouped with "soft" Gaussian factors also belong to Gaussian. With the EM Gaussian messages from the E-step, the max-product message passing in the M-step factor graph can also be realised using the GMP technique. The above lead to pure GMP for EM algorithm.

We summarise the computation rules of GMP backwards through a multiplier node [59] in Table 4.1 and Table 4.2. It turns out that the EM message $\mathrm{e}^{\eta(\theta)}$ is always Gaussian with mean $\overleftarrow{m}_\theta$ and weighted matrix $\overleftarrow{W}_\theta$. In Table 4.1, X and θ are real column vectors, and $S = \theta^T X$ is a scalar. $N(m, \sigma^2)$ denotes a scalar Gaussian factor with mean m and variance σ^2. In Table 4.2, we have a multiplier $U = A(\theta)X$, where $A(\theta)$ is a matrix which depends on θ, grouped with $Y = U + Z$, where Z is a zero-mean Gaussian noise with covariance matrix $V_Z = W_Z^{-1}$ (or variance σ_Z^2 for scalar). The other variables in both Table 4.1 and Table 4.2 are Gaussian with mean vectors and covariance matrices which can be computed using the GMP rules in [52]. Table 4.2 only shows the case of scalar θ times vector X, and other cases are provided in [59].

One of the attractive advantages of the message passing EM algorithm is that tabulated message passing computation rules provide simplification of the

Table 4.1: Computation Rules for Gaussian Message Passing Backwards Through a Multiplier.

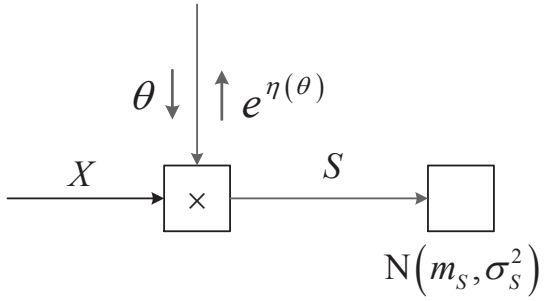

The EM message $e^{\eta(\theta)}$ is Gaussian with

$$\overleftarrow{W}_\theta = \frac{V_X + m_X m_X^T}{\sigma_S^2} \tag{4.9}$$

$$\overleftarrow{W}_\theta \overleftarrow{m}_\theta = \frac{m_X m_S}{\sigma_S^2} \tag{4.10}$$

where

$$V_X^{-1} = W_X = \overrightarrow{W}_X + \theta\theta^T/\sigma_S^2 \tag{4.11}$$

$$W_X m_X = \overrightarrow{W}_X \overrightarrow{m}_X + \theta m_S/\sigma_S^2 \tag{4.12}$$

Table 4.2: Computation Rules for Gaussian Backward EM Message Through Multiplier Node (scalar θ times vector X).

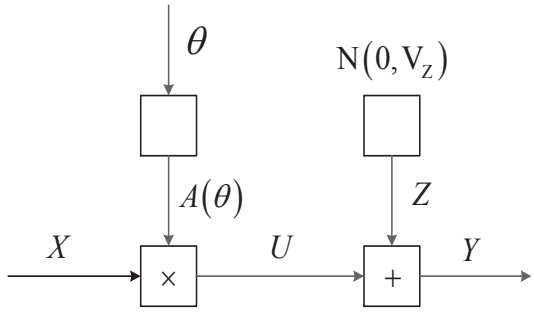

Scalar θ times column vector X, $A(\theta) = \theta$

$$1/\overleftarrow{\sigma}_\theta^2 = \mathrm{tr}(W_Z V_X) + m_X^T W_Z m_X \tag{4.13}$$

$$\overleftarrow{m}_\theta/\overleftarrow{\sigma}_\theta^2 = \mathrm{tr}(W_Z V_{XY^T}) + m_X^T W_Z m_Y \tag{4.14}$$

where

$$V_{XY^T} = \overrightarrow{V}_X A(\hat{\theta})^T \tilde{W}_Y \overleftarrow{V}_Y \tag{4.15}$$

derivation of message passing algorithms [52, 59].

4.3 EM Based Time-Varying Channel Estimation Using Gaussian Message Passing

We consider the flat Rayleigh fading channels. The same models of (3.25) and (3.29) are used to represent the received signal and the AR(1) model, respectively. With an FFG representation of the fading channel approximated by an AR(1) model, we exploit the EM GMP algorithm to iteratively estimate channel coefficients and AR(1) model coefficients, where the channel coefficients $\{h_k\}$ are treated as hidden variables, and the AR(1) model coefficients α and g are treated as unknown parameters. The FFG of the system model described by (3.25) and (3.29) is shown in Fig. 4.2, where we partition the overall factor graph into two subgraphs: E-step factor graph and M-step factor graph. Note that all the variables in Fig. 4.2 are scalars. Following the convention in [52] and [59], we use the same notations stated in Chapter 3 to denote the means and variances of messages with directions.

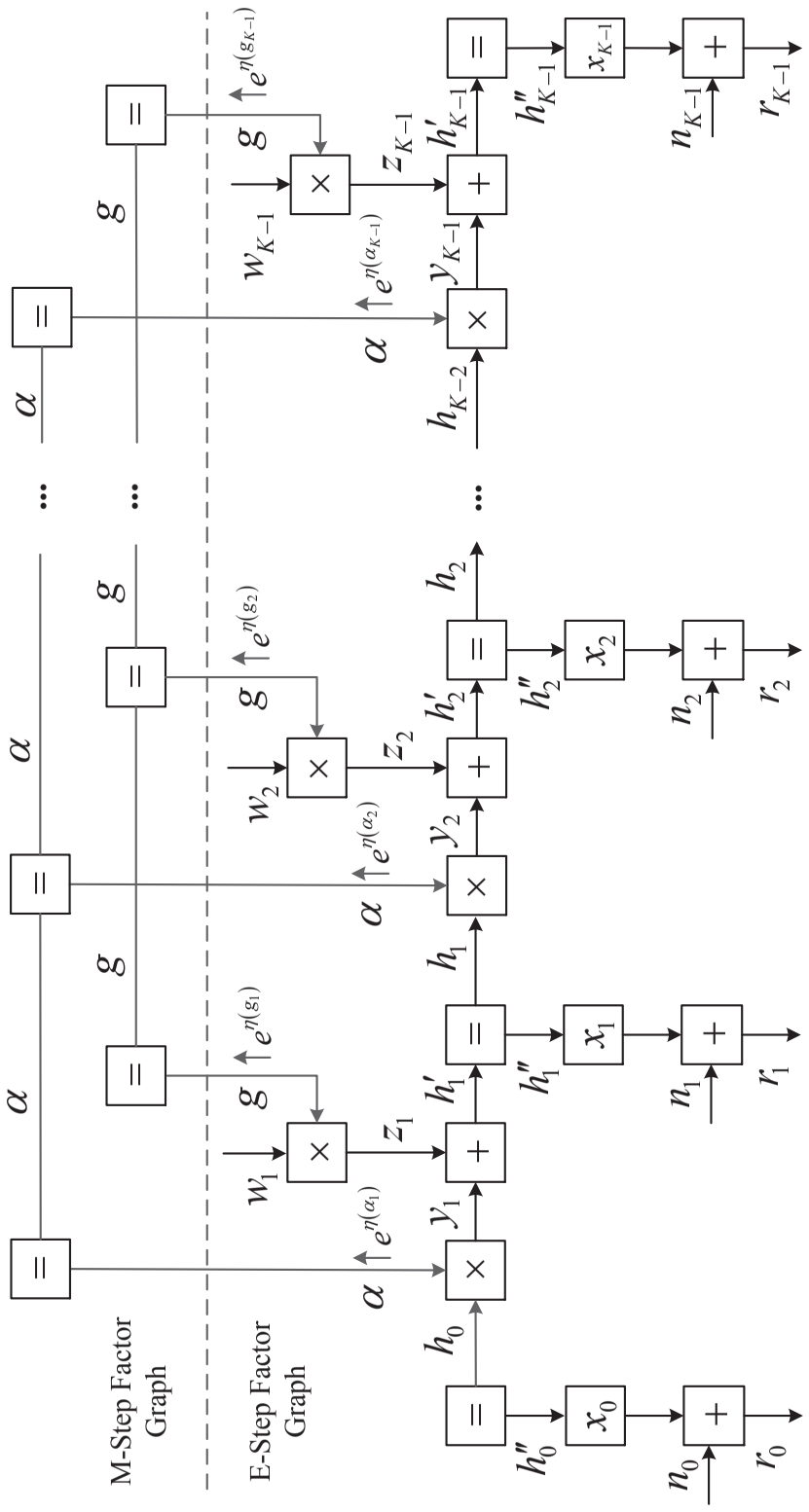

Figure 4.2: The factor graph of the Rayleigh fading channel with AR(1) model for EM algorithm

The implementations of the E-step and M-step for the ith iteration of the proposed EM approach are detailed in the following:

- E-Step Implementation:

  In this step, we aim to compute the EM Gaussian messages of the multiplier nodes corresponding to AR(1) model coefficients α and g respectively. Firstly, plugged with the messages of $\left\{\hat{\alpha}_k^{(i-1)}\right\}$ and $\left\{\hat{g}_k^{(i-1)}\right\}$ (the estimates of $\{\alpha\}$ and $\{g\}$ in the (i-1)th EM iteration), we employ the GMP techniques on the E-step factor graph through a forward and backward recursion to calculate the means and variances of $\{h_k\}, \{y_k\}, \left\{h'_k\right\}$ in both directions, where $k = 1, \cdots, K-1$.

  Forward Recursion: In this process, we need to compute $\left\{\overrightarrow{m}_{y_k}, \overrightarrow{V}_{y_k}\right\}$, $\left\{\overrightarrow{m}_{h'_k}, \overrightarrow{V}_{h'_k}\right\}$ and $\left\{\overrightarrow{m}_{h_k}, \overrightarrow{V}_{h_k}\right\}$ in the kth building block. Assume that $\left\{\overrightarrow{m}_{h_{k-1}}, \overrightarrow{V}_{h_{k-1}}\right\}$ are available from the building blocks left to the kth building block. Using the GMP updating rules in [52], $\left\{\overrightarrow{m}_{y_k}, \overrightarrow{V}_{y_k}\right\}$ can be calculated as

$$\overrightarrow{m}_{y_k} = \hat{\alpha}_k^{(i-1)} \overrightarrow{m}_{h_{k-1}} \tag{4.16a}$$

$$\overrightarrow{V}_{y_k} = (\hat{\alpha}_k^{(i-1)})^2 \overrightarrow{V}_{h_{k-1}}, \tag{4.16b}$$

  and $\left\{\overrightarrow{m}_{h'_k}, \overrightarrow{V}_{h'_k}\right\}$ can be computed as

$$\overrightarrow{m}_{h'_k} = \overrightarrow{m}_{y_k} \tag{4.17a}$$

$$\overrightarrow{V}_{h'_k} = \overrightarrow{V}_{y_k} + (\hat{g}_k^{(i-1)})^2. \tag{4.17b}$$

  The message $\left\{\overrightarrow{V}_{h_k}, \overrightarrow{m}_{h_k}\right\}$ can be computed as

$$\overrightarrow{V}_{h_k} = \left(\overrightarrow{V}_{h'_k}^{-1} + \overleftarrow{V}_{h''_k}^{-1}\right)^{-1} \tag{4.18a}$$

$$\overrightarrow{m}_{h_k} = \overrightarrow{V}_{h_k}\left(\overrightarrow{m}_{h'_k} \overrightarrow{V}_{h'_k}^{-1} + \overleftarrow{m}_{h''_k} \overleftarrow{V}_{h''_k}^{-1}\right) \tag{4.18b}$$

with

$$\overleftarrow{V}_{h_k''} = \frac{\overrightarrow{V}_{n_k}}{x_k^2} = \sigma_n^2 \tag{4.19a}$$

$$\overleftarrow{m}_{h_k''} = \frac{\overleftarrow{m}_{r_k}}{x_k} = r_k. \tag{4.19b}$$

According to the GMP rules in [52], we have $\overrightarrow{m}_{h_0} = r_0$ and $\overrightarrow{V}_{h_0} = \sigma_n^2$ for the first building block.

Backward Recursion: In this process, we need to compute $\left\{\overleftarrow{m}_{h_k'}, \overleftarrow{V}_{h_k'}\right\}$ and $\left\{\overleftarrow{m}_{h_{k-1}}, \overleftarrow{V}_{h_{k-1}}\right\}$ in the kth building block. Assume that $\left\{\overleftarrow{m}_{h_k}, \overleftarrow{V}_{h_k}\right\}$ are available from the building blocks right to the kth building block. Using the GMP updating rules in [52], $\left\{\overleftarrow{V}_{h_k'}, \overleftarrow{m}_{h_k'}\right\}$ can be calculated as

$$\overleftarrow{V}_{h_k'} = \left(\overleftarrow{V}_{h_k}^{-1} + \overleftarrow{V}_{h_k''}^{-1}\right)^{-1} \tag{4.20a}$$

$$\overleftarrow{m}_{h_k'} = \overleftarrow{V}_{h_k'}\left(\overleftarrow{m}_{h_k}\overleftarrow{V}_{h_k}^{-1} + \overleftarrow{m}_{h_k''}\overleftarrow{V}_{h_k''}^{-1}\right), \tag{4.20b}$$

where $\left\{\overleftarrow{V}_{h_k''}, \overleftarrow{m}_{h_k''}\right\}$ are given by (4.19a) and (4.19b). According to the GMP rules in [52], we have $\overleftarrow{m}_{h_{k'}} = r_{K-1}$ and $\overleftarrow{V}_{h_{k'}} = \sigma_n^2$ for the $(K-1)$th building block. The message $\left\{\overleftarrow{m}_{h_{k-1}}, \overleftarrow{V}_{h_{k-1}}\right\}$ can be computed as

$$\overleftarrow{m}_{h_{k-1}} = \frac{\overleftarrow{m}_{h_k'}}{\hat{\alpha}_k^{(i-1)}} \tag{4.21a}$$

$$\overleftarrow{V}_{h_{k-1}} = \frac{\overleftarrow{V}_{h_k'} + \left(\hat{g}_k^{(i-1)}\right)^2}{\left(\hat{\alpha}_k^{(i-1)}\right)^2}. \tag{4.21b}$$

The Marginal Messages: By combining the forward and backward messages, the marginal messages $\{V_{h_k}, m_{h_k}\}$ in the kth building block are given by

$$V_{h_k} = \left(\overrightarrow{V}_{h_k}^{-1} + \overleftarrow{V}_{h_k}^{-1}\right)^{-1} \tag{4.22a}$$

$$m_{h_k} = V_{h_k}\left(\overrightarrow{m}_{h_k}\overrightarrow{V}_{h_k}^{-1} + \overleftarrow{m}_{h_k}\overleftarrow{V}_{h_k}^{-1}\right) \tag{4.22b}$$

where m_{h_k} is used as the estimate of h_k.

With the incoming messages $\left\{\overrightarrow{m}_{h_k}, \overrightarrow{V}_{h_k}\right\}$, $\left\{\overleftarrow{m}_{h'_{k+1}}, \overleftarrow{V}_{h'_{k+1}}\right\}$ and $\left\{\hat{\alpha}^{(i-1)}\right\}$, we compute the outgoing EM messages $\left\{\overleftarrow{W}_{\alpha_k}, \overleftarrow{W}_{\alpha_k}\overleftarrow{m}_{\alpha_k}\right\}$ for $\{\alpha_k\}$ of the multiplier nodes. According to rules (4.13), (4.14) and (4.15) in Table 4.2, the EM message for α_k can be calculated as

$$\overleftarrow{W}_{\alpha_k} = V_{h_k} + m_{h_k} m_{h_k} \tag{4.23a}$$

$$\overleftarrow{W}_{\alpha_k}\overleftarrow{m}_{\alpha_k} = V_{h_k h'^{T}_{k+1}} + m_{h_k} m_{h'_{k+1}}, \tag{4.23b}$$

where

$$V_{h_k h'^{T}_{k+1}} = V_{h_k}\hat{\alpha}_k^{(i-1)}\tilde{W}_{h'_{k+1}} V_{h'^{T}_{k+1}} \tag{4.24a}$$

$$\tilde{W}_{h'_{k+1}} = \left(\overrightarrow{V}_{h'_{k+1}} + \overleftarrow{V}_{h'_{k+1}}\right)^{-1}. \tag{4.24b}$$

With the incoming messages $\left\{\overrightarrow{m}_{y_k}, \overrightarrow{V}_{y_k}\right\}$ and $\left\{\overleftarrow{m}_{h'_k}, \overleftarrow{V}_{h'_k}\right\}$, we can form scalar Gaussian factors with mean and variance of $\{m_{z_k}, V_{z_k}\}$ connected to the edge with variable z_k to replace the adder nodes in Fig. 4.2. Using rules in Table 3.1, $\{m_{z_k}, V_{z_k}\}$ can be computed as

$$m_{z_k} = \overleftarrow{m}_{h'_k} - \overrightarrow{m}_{y_k} \tag{4.25a}$$

$$V_{z_k} = \overrightarrow{V}_{y_k} + \overleftarrow{V}_{h'_k}. \tag{4.25b}$$

With the incoming messages $\left\{\overrightarrow{m}_{w_k}, \overrightarrow{V}_{w_k}\right\}$, $\{m_{z_k}, V_{z_k}\}$ and $\left\{\hat{g}^{(i-1)}\right\}$, we compute the outgoing EM messages $\left\{\overleftarrow{W}_{g_k}, \overleftarrow{W}_{g_k}\overleftarrow{m}_{g_k}\right\}$ for $\{g_k\}$ of the multiplier nodes. According to rules (4.9)-(4.12) in Table 4.1, the EM messages for g_k can be calculated as

$$\overleftarrow{W}_{g_k} = V_{w_k} + \frac{m_{w_k} m_{w_k}}{V_{z_k}} \tag{4.26a}$$

$$\overleftarrow{W}_{g_k}\overleftarrow{m}_{g_k} = \frac{m_{w_k} m_{z_k}}{V_{z_k}}, \tag{4.26b}$$

where

$$V_{w_k} = \frac{V_{z_k}}{V_{z_k} + \hat{g}^{2^{(i-1)}}} \tag{4.27a}$$

$$m_{w_k} = \frac{\hat{g}^{(i-1)}}{V_{z_k} + \hat{g}^{2^{(i-1)}}} m_{z_k}. \tag{4.27b}$$

- M-Step Implementation:

  In this step, we aim to obtain the new estimates for $\{\alpha_k\}$ and $\{g_k\}$ by running GMP with message computation rules for the equality nodes in the M-step factor graph in Fig. 4.2. The exact calculation involves forward and backward recursions which incur unnecessary computations of some products. As the M-step factor graph in Fig. 4.2 only includes equality nodes, the marginal mean scalar of $\{\alpha_k\}$ and $\{g_k\}$ can be simplified as

$$m_{\alpha_k} = \frac{\sum_{k=1}^{K-1} \overleftarrow{W}_{\alpha_k} \overleftarrow{m}_{\alpha_k}}{\sum_{k=1}^{K-1} \overleftarrow{W}_{\alpha_k}} \tag{4.28a}$$

$$m_{g_k} = \frac{\sum_{k=1}^{K-1} \overleftarrow{W}_{g_k} \overleftarrow{m}_{g_k}}{\sum_{k=1}^{K-1} \overleftarrow{W}_{g_k}}. \tag{4.28b}$$

  The new estimates $\alpha_k = m_{\alpha_k}$ and $g_k = m_{g_k}$ where $k = 1, 2, \cdots, K-1$, will be employed by the E-step in the next iteration.

In the above approach, it requires an initialisation of α and g for the first iteration, where we use the received signal with (3.36) and (3.37) for initialisation. The proposed EM GMP approach has similar complexity as the EM approach in [11] per iteration.

4.4 Simulation Results

The system settings are the same as those in Chapter 3, where pilots symbols are used for channel estimation. Fig. 4.3 shows the MSE performance of the proposed

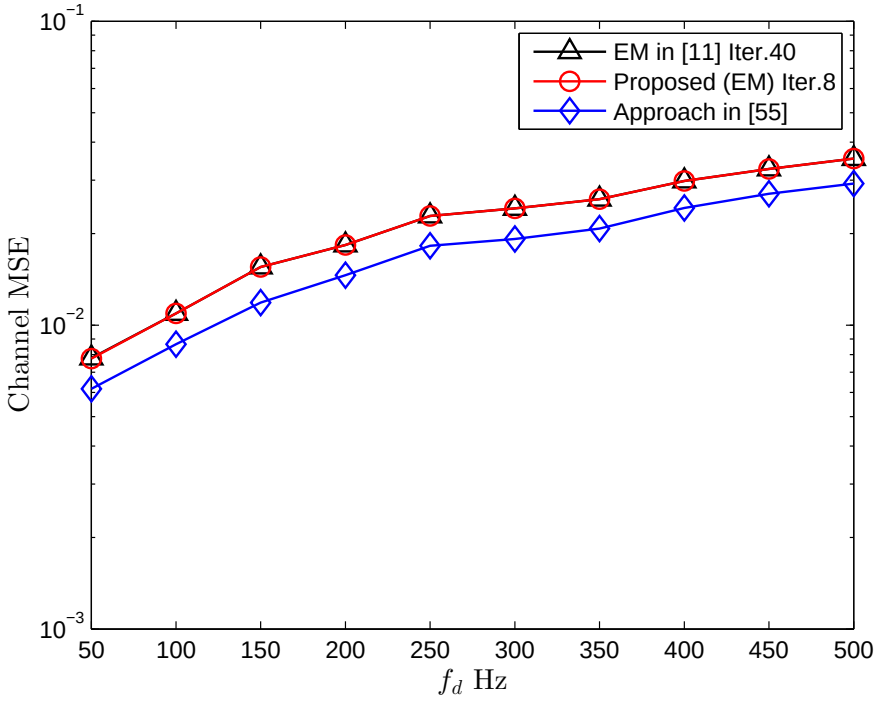

Figure 4.3: MSE performance of channel estimation for $K = 100$ and SNR= 10dB

EM approach, the EM approach in [11] and the approach in [55]. It can be seen that the proposed EM approach has the same performance with the EM approach in [11]. The proposed approach is very close to the performance of the approach in [55], where the approach in [55] assumes the optimal AR(1) model is known.

Fig. 4.4 and Fig. 4.5 show the convergence rate of the proposed EM approach and the EM approach in [11] with $f_d = 50$ Hz and $f_d = 500$ Hz respectively. It can been seen that the proposed EM approach achieves considerable performance improvement in terms of convergence rate, where the maximum iteration number of the proposed approach is 8 and the maximum iteration number of the EM approach in [11] is 40 for $f_d = 50$ Hz. Therefore, the total complexity of the proposed EM approach is much lower than that of the EM approach in [11].

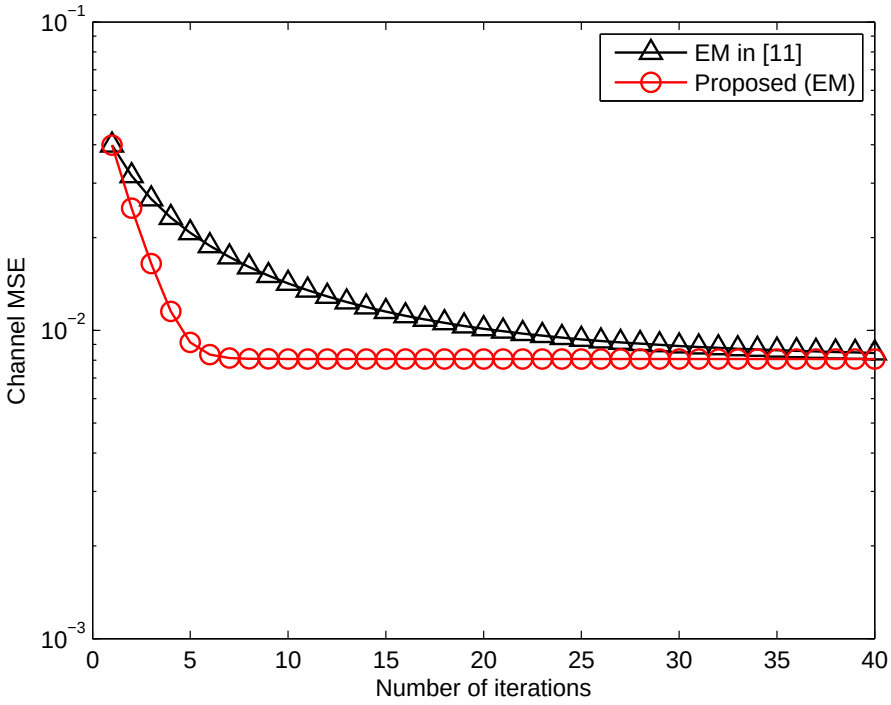

Figure 4.4: MSE versus number of iterations for channel estimation with $f_d = 50$ Hz, $K = 100$ and SNR=10dB

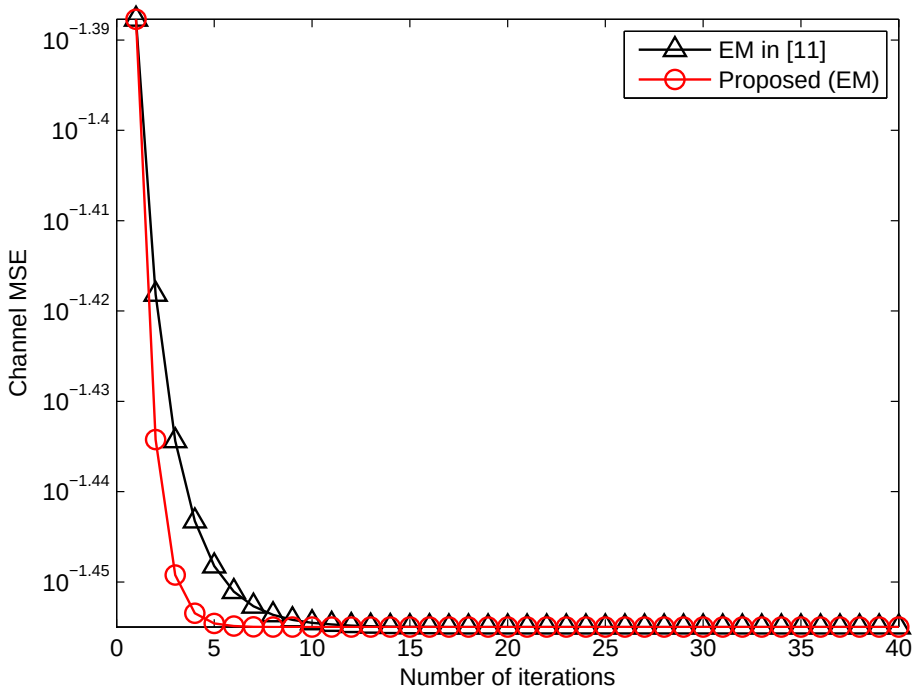

Figure 4.5: MSE versus number of iterations for channel estimation with $f_d = 500$ Hz, $K = 100$ and SNR=10dB

4.5 Conclusion

In this Chapter, we devised a time-varying channel estimation approach using message passing based EM algorithm. With a FFG representation of the Rayleigh fading channel approximated by an AR(1) model, we treat the channel coefficients as hidden data and treat the AR(1) model coefficients as unknown parameters. By employing the GMP techniques for the EM algorithm, we developed a joint channel estimation and AR model coefficients estimation approach, where the proposed approach achieves much faster convergence speed and lower complexity compared with the conventional EM approach. Note that the Doppler spread can be extracted from the estimated AR(1) model coefficients [11].

Chapter 5

Conclusions and Future Work

5.1 Conclusions

The objective of this thesis is to design efficient algorithms for Doppler spread estimation in high mobility wireless communication systems. After introducing the properties of time-varying fading channels and reviewing some existing Doppler spread estimation approaches, motivated by the advantages of joint Doppler spread and channel estimation, we proposed two low-complexity algorithms using Gaussian message passing (GMP) techniques. We summarise this thesis as follows.

In Chapter 3, we proposed a new low-complexity iterative approach to joint Doppler spread and channel estimation over Rayleigh fading channels. Through an iterative process between two devised estimators, i.e., an autocorrelation function (ACF) based Doppler spread estimator with an ACF lag selection mechanism and a GMP based channel estimator with a Forney-style factor graph (FFG) representation of an optimised AR(1) channel model, we achieve similar or better

performance with lower complexity compared to existing joint Doppler spread and channel estimation approaches.

In Chapter 4, using a FFG to represent the Rayleigh fading channels described by an AR(1) model, we developed the GMP technique for EM algorithm to joint channel and AR(1) model coefficients estimation, where the Doppler spread can be extracted from the estimated AR(1) model coefficients. The proposed EM-GMP approach has the same performance with the conventional EM approach, but the convergence speed is much faster.

To sum up, in this thesis, we mainly focus on joint Doppler spread and channel estimation using GMP techniques. Compared to existing approaches, we have shown the proposed approaches achieves better performance over a wide range of maximum Doppler frequency with even lower complexity.

5.2 Future Work

In this thesis, we mainly investigate the joint Doppler spread and channel estimation approaches over flat Rayleigh fading channels. In a practical radio wave propagation environment, such as rural area where the high speed railway systems are operated, the scattering is often nonisotropic and the receiver may have a line-of-sight component. Thus, the fading channel is more suitable to be modeled as a Rician fading channel. It is necessary to investigate Doppler spread estimation for Rician fading channels. This thesis assumes that the Rayleigh fading channel is due to Jake's model and the knowledge of channel PSD is the U-shape. It is interesting to research robust Doppler spread estimation that does not need the prior knowledge of Doppler spectrum. As the future wireless communication

systems aims at providing reliable data transmission to support broadband communication even under high mobility environments, frequency selective channels have to be taken into account for joint channel and Doppler spread estimation. In addition, the proposed joint channel and Doppler spread estimation approach may be incorporated into turbo equalisation for joint channel, Doppler spread and detection. We list the some several possible topics for future work as follows:

- Joint Doppler spread and channel estimation for Rician fading channels,
- Joint Doppler spread and channel estimation for time-varying frequency selective fading channels,

  and
- Joint channel, Doppler spread estimation and data detection.

References

[1] P. Fan, E. Panayirci, H. V. Poor, and P. T. Mathiopoulos, "Special issue on broadband mobile communications at very high speeds," *EURASIP Journal on Wireless Communications and Networking*, vol. 2012, no. 1, pp. 1–3, 2012.

[2] T. S. Rappaport *et al.*, *Wireless communications: principles and practice*. Prentice Hall PTR New Jersey, 1996, vol. 2.

[3] L. Krasny, H. Arslan, D. Koilpillai, and S. Chennakeshu, "Doppler spread estimation in mobile radio systems," *IEEE communications letters*, vol. 5, no. 5, pp. 197–199, 2001.

[4] T. Yucek, R. M. Tannious, and H. Arslan, "Doppler spread estimation for wireless OFDM systems," in *IEEE/Sarnoff Symposium on Advances in Wired and Wireless Communication*. IEEE, 2005, pp. 233–236.

[5] A. Abdi, H. Zhang, and C. Tepedelenlioglu, "A unified approach to the performance analysis of speed estimation techniques in mobile communication," *IEEE Transactions on Communications*, vol. 56, no. 1, pp. 126–135, 2008.

[6] H. Zhang and A. Abdi, "Cyclostationarity-based Doppler spread estimation in mobile fading channels," *IEEE Transactions on Communications*, vol. 57, no. 4, pp. 1061–1067, 2009.

[7] C. W. Sung and W. S. Wong, "User speed estimation and dynamic channel allocation in hierarchical cellular system," in *IEEE 44th Vehicular Technology Conference*. IEEE, 1994, pp. 91–95.

[8] G. L. Stüber, *Principles of mobile communication*. Springer, 2011.

[9] J. M. Holtzman and A. Sampath, "Adaptive averaging methodology for handoffs in cellular systems," *IEEE Transactions on Vehicular Technology*, vol. 44, no. 1, pp. 59–66, 1995.

[10] K.-J. Yang, C.-L. Wang, and Y.-R. Tsai, "Joint channel and Doppler spread estimation over time-varying flat-fading channels," in *IEEE 75th Vehicular Technology Conference*. IEEE, 2012, pp. 1–5.

[11] M. Nissila and S. Pasupathy, "Joint estimation of carrier frequency offset and statistical parameters of the multipath fading channel," *IEEE Transactions on Communications*, vol. 54, no. 6, pp. 1038–1048, 2006.

[12] W. C. Jakes and D. C. Cox, *Microwave mobile communications*. Wiley-IEEE Press, 1994.

[13] C. Tepedelenlioglu and G. B. Giannakis, "On velocity estimation and correlation properties of narrow-band mobile communication channels," *IEEE Transactions on Vehicular Technology*, vol. 50, no. 4, pp. 1039–1052, 2001.

[14] A. Goldsmith, *Wireless communications*. Cambridge university press, 2005.

[15] S. S. Haykin and M. Moher, *Modern wireless communication*. Prentice Hall, 2004.

[16] Y. R. Zheng and C. Xiao, "Improved models for the generation of multiple uncorrelated Rayleigh fading waveforms," *IEEE Communications Letters*, vol. 6, no. 6, pp. 256–258, 2002.

[17] R. Clarke, "A statistical theory of mobile-radio reception," *Bell system technical journal*, vol. 47, no. 6, pp. 957–1000, 1968.

[18] M. D. Austin and G. Stüber, "Velocity adaptive handoff algorithms for microcellular systems," *IEEE Transactions on Vehicular Technology*, vol. 43, no. 3, pp. 549–561, 1994.

[19] A. Abdi and M. Kaveh, "A new velocity estimator for cellular systems based on higher order crossings," in *Conference Record of the Thirty-Second Asilomar Conference on Signals, Systems and Computers*, vol. 2. IEEE, 1998, pp. 1423–1427.

[20] C. Tepedelenlioğlu, A. Abdi, G. B. Giannakis, and M. Kaveh, "Estimation of Doppler spread and signal strength in mobile communications with applications to handoff and adaptive transmission," *Wireless Communications and Mobile Computing*, vol. 1, no. 2, pp. 221–242, 2001.

[21] G. Park, D. Hong, and C. Kang, "Level crossing rate estimation with Doppler adaptive noise suppression technique in frequency domain," in *IEEE 58th Vehicular Technology Conference*, vol. 2. IEEE, 2003, pp. 1192–1195.

[22] X. Chen, P.-S. Kildal, and J. Carlsson, "Determination of maximum Doppler shift in reverberation chamber using level crossing rate," in *Proceedings of the 5th European Conference on Antennas and Propagation (EUCAP)*. IEEE, 2011, pp. 62–65.

[23] K. Baddour and N. Beaulieu, "Nonparametric doppler spread estimation for flat fading channels," in *IEEE Conference on Wireless Communications and Networking (WCNC)*, vol. 2, March 2003, pp. 953–958 vol.2.

[24] S. Mohanty, "VEPSD: a novel velocity estimation algorithm for next-generation wireless systems," *IEEE Transactions on Wireless Communications*, vol. 4, no. 6, pp. 2655–2660, Nov 2005.

[25] H. Zhang and A. Abdi, "A robust mobile speed estimator in fading channels: performance analysis and experimental results," in *IEEE Global Telecommunications Conference (GLOBECOM)*, vol. 5, Dec 2005, pp. 5 pp.–2573.

[26] K. Muralidhar, K. H. Li, and K. Hari, "Iterative Kalman-AR method for Doppler spread estimation in flat fading channels," in *IEEE 18th International Symposium on Personal, Indoor and Mobile Radio Communications*. IEEE, 2007, pp. 1–5.

[27] K. D. Anim-Appiah, "On generalized covariance-based velocity estimation," *IEEE Transactions on Vehicular Technology*, vol. 48, no. 5, pp. 1546–1557, 1999.

[28] W. Sheng and S. D. Blostein, "SNR-independent velocity estimation for mobile cellular communications systems," in *IEEE International Conference on*

Acoustics, Speech, and Signal Processing (ICASSP), vol. 3. IEEE, 2002, pp. III–2469.

[29] J. Cai, W. Song, and Z. Li, "Doppler spread estimation for mobile OFDM systems in Rayleigh fading channels," *IEEE Transactions on Consumer Electronics*, vol. 49, no. 4, pp. 973–977, 2003.

[30] O. Mauritz, "A hybrid method for Doppler spread estimation," in *IEEE 59th Vehicular Technology Conference*, vol. 2. IEEE, 2004, pp. 962–965.

[31] G. Park, S. Nam, T. Yu, D. Hong, and C. Kang, "A modified covariance-based mobile velocity estimation method for Rician fading channels," *IEEE Communications Letters*, vol. 9, no. 8, pp. 706–708, 2005.

[32] K. E. Baddour and N. C. Beaulieu, "Robust Doppler spread estimation in nonisotropic fading channels," *IEEE Transactions on Wireless Communications*, vol. 4, no. 6, pp. 2677–2682, 2005.

[33] P.-Y. Chen and H.-J. Li, "An iterative algorithm for Doppler spread estimation in LOS environments," *IEEE Transactions on Wireless Communications*, vol. 5, no. 6, pp. 1223–1228, 2006.

[34] L. Qiaoli, C. Wei, X. Tao, and L. Biqi, "A Doppler spread estimator design for mobile OFDM systems," in *IEEE Singapore International Conference on Communication Systems*. IEEE, 2008, pp. 1046–1049.

[35] Y. Zheng and C. Xiao, "Mobile speed estimation for broadband wireless communications over Rician fading channels," *IEEE Transactions on Wireless Communications*, vol. 8, no. 1, pp. 1–5, Jan 2009.

[36] M. Souden, S. Affes, J. Benesty, and R. Bahroun, "Robust Doppler spread estimation in the presence of a residual carrier frequency offset," *IEEE Transactions on Signal Processing*, vol. 57, no. 10, pp. 4148–4153, 2009.

[37] A. Singhapan, K. Naito, K. Mori, P. Boonsrimuang, and H. Kobayashi, "Doppler frequency spread estimation for OFDM systems in time-varying fading channel," in *International Conference on Electrical Engineering/Electronics, Computer, Telecommunications and Information Technology (ECTI-CON)*. IEEE, 2012, pp. 1–4.

[38] P. Huang, D. Rajan, and J. Camp, "An autoregressive Doppler spread estimator for fading channels," *IEEE Wireless Communications Letters*, vol. 2, no. 6, pp. 655–658, December 2013.

[39] H. Hansen, S. Affes, and P. Mermelstein, "A Rayleigh Doppler frequency estimator derived from maximum likelihood theory," in *IEEE Workshop on Signal Processing Advances in Wireless Communications*. IEEE, 1999, pp. 382–386.

[40] A. Dogandzic and B. Zhang, "Estimating Jakes' Doppler power spectrum parameters using the whittle approximation," *IEEE Transactions on Signal Processing*, vol. 53, no. 3, pp. 987–1005, 2005.

[41] Y.-S. Choi, O. Can Ozdural, H. Liu, and S. Alamouti, "A maximum likelihood Doppler frequency estimator for OFDM systems," in *IEEE International Conference on Communications (ICC)*, vol. 10. IEEE, 2006, pp. 4572–4576.

[42] T. Yuh-Ren and Y. Kai-Jie, "Approximate ML Doppler spread estimation over

flat Rayleigh fading channels," *IEEE Signal Processing Letters*, vol. 16, no. 11, pp. 1007–1010, 2009.

[43] Y.-R. Tsai, K.-J. Yang, C.-H. Tsai, and C.-L. Wang, "Low-complexity ML Doppler spread estimation for OFDM systems," in *IEEE Vehicular Technology Conference (VTC Fall)*. IEEE, 2011, pp. 1–5.

[44] F. Bellili and S. Affes, "A low-cost and robust maximum likelihood Doppler spread estimator," in *IEEE Global Communications Conference (GLOBECOM)*. IEEE, 2013, pp. 4325–4330.

[45] Q. Guo, L. Ping, and D. Huang, "A low-complexity iterative channel estimation and detection technique for doubly selective channels," *IEEE Transactions on Wireless Communications*, vol. 8, no. 8, pp. 4340–4349, August 2009.

[46] Q. Guo and D. Huang, "GMP-based channel estimation for single-carrier transmissions over doubly selective channels," *IEEE Signal Processing Letters*, vol. 17, no. 1, pp. 8–11, Jan 2010.

[47] N. Geng, X. Yuan, and L. Ping, "Dual-Diagonal LMMSE channel estimation for OFDM systems," *IEEE Transactions on Signal Processing*, vol. 60, no. 9, pp. 4734–4746, Sept 2012.

[48] A. Movahedian and M. McGuire, "Estimation of fast-fading channels for turbo receivers with high-order modulation," *IEEE Transactions on Vehicular Technology*, vol. 62, no. 2, pp. 667–678, Feb 2013.

[49] K. E. Baddour and N. C. Beaulieu, "Autoregressive modeling for fading

channel simulation," *IEEE Transactions on Wireless Communications*, vol. 4, no. 4, pp. 1650–1662, 2005.

[50] R. H. Shumway and D. S. Stoffer, "An approach to time series smoothing and forecasting using the EM algorithm," *Journal of time series analysis*, vol. 3, no. 4, pp. 253–264, 1982.

[51] S. M. Kay, *Fundamentals of statistical signal processing: estimation theory*. Prentice-Hall, Inc., 1993.

[52] H.-A. Loeliger, J. Dauwels, J. Hu, S. Korl, P. Li, and F. R. Kschischang, "The factor graph approach to model-based signal processing," *Proceedings of the IEEE*, vol. 95, no. 6, pp. 1295–1322, 2007.

[53] H.-A. Loeliger, J. Hu, S. Korl, Q. Guo, and L. Ping, "Gaussian message passing on linear models: An update," in *International Symposium on Turbo Codes Related Topics*, April 2006, pp. 1–7.

[54] H.-A. Loeliger, "An introduction to factor graphs," *IEEE Signal Processing Magazine*, vol. 21, no. 1, pp. 28–41, Jan 2004.

[55] S. Ghandour-Haidar, L. Ros, and J.-M. Brossier, "On the use of first-order autoregressive modeling for Rayleigh flat fading channel estimation with Kalman filter," *Signal Processing*, vol. 92, no. 2, pp. 601–606, 2012.

[56] Q. Dai and E. Shwedyk, "Detection of bandlimited signals over frequency selective Rayleigh fading channels," *IEEE Transactions on Comuncations*, vol. 42, no. 234, pp. 941–950, 1994.

[57] A. Barbieri, A. Piemontese, and G. Colavolpe, "On the ARMA approximation for fading channels described by the Clarke model with applications to Kalman-based receivers," *IEEE Transactions on Wireless Communications*, vol. 8, no. 2, pp. 535–540, 2009.

[58] H. S. Wang and P.-C. Chang, "On verifying the first-order markovian assumption for a rayleigh fading channel model," *IEEE Transactions on Vehicular Technology*, vol. 45, no. 2, pp. 353–357, 1996.

[59] J. Dauwels, A. Eckford, S. Korl, and H.-A. Loeliger, "Expectation maximization as message passing-part i: Principles and gaussian messages," *arXiv preprint arXiv:0910.2832*, 2009.